Article

Current Biology

The WIP6 transcription factor *TOO MANY LATERALS* specifies vein type in C_4 and C_3 grass leaves

Highlights

- Function of WIP6 ortholog *TML* is conserved in maize and rice
- *TML* is expressed in procambial cells during early leaf vein development
- *tml* mutants develop large lateral veins in places where smaller veins should form
- TML function suppresses lateral vein development in a subset of procambial initials

Authors

Daniela Vlad, Maricris Zaidem, Chiara Perico, Olga Sedelnikova, Samik Bhattacharya, Jane A. Langdale

Correspondence

jane.langdale@biology.ox.ac.uk

In brief

Vlad et al. discover a conserved mechanism that determines whether procambial stem cells in grass leaf primordia will develop into large lateral or smaller intermediate veins. The mechanism is revealed through the analysis of mutants defective in the activity of a zinc finger transcription factor of the WIP6 family that is named TOO MANY LATERALS.

Vlad et al., 2024, Current Biology *34*, 1670–1686
April 22, 2024
https://doi.org/10.1016/j.cub.2024.03.007

CellPress

CellPress
OPEN ACCESS

Current Biology

Article

The WIP6 transcription factor *TOO MANY LATERALS* specifies vein type in C_4 and C_3 grass leaves

Daniela Vlad,[1] Maricris Zaidem,[1] Chiara Perico,[1] Olga Sedelnikova,[1,3] Samik Bhattacharya,[2] and Jane A. Langdale[1,4,*]
[1]Department of Biology, University of Oxford, South Parks Rd, Oxford OX1 3RB, UK
[2]Resolve BioSciences GmbH, Alfred-Nobel-Straße 10, 40789 Monheim am Rhein, Germany
[3]Present address: Syngenta Jealott's Hill International Research Centre, Bracknell RG42 6EY, UK
[4]Lead contact
*Correspondence: jane.langdale@biology.ox.ac.uk
https://doi.org/10.1016/j.cub.2024.03.007

SUMMARY

Grass leaves are invariantly strap shaped with an elongated distal blade and a proximal sheath that wraps around the stem. Underpinning this shape is a scaffold of leaf veins, most of which extend in parallel along the proximo-distal leaf axis. Differences between species are apparent both in the vein types that develop and in the distance between veins across the medio-lateral leaf axis. A prominent engineering goal is to increase vein density in leaves of C_3 photosynthesizing species to facilitate the introduction of the more efficient C_4 pathway. Here, we discover that the WIP6 transcription factor TOO MANY LATERALS (TML) specifies vein rank in both maize (C_4) and rice (C_3). Loss-of-function *tml* mutations cause large lateral veins to develop in positions normally occupied by smaller intermediate veins, and *TML* transcript localization in wild-type leaves is consistent with a role in suppressing lateral vein development in procambial cells that form intermediate veins. Attempts to manipulate TML function in rice were unsuccessful because transgene expression was silenced, suggesting that precise *TML* expression is essential for shoot viability. This finding may reflect the need to prevent the inappropriate activation of downstream targets or, given that transcriptome analysis revealed altered cytokinin and auxin signaling profiles in maize *tml* mutants, the need to prevent local or general hormonal imbalances. Importantly, rice *tml* mutants display an increased occupancy of veins in the leaf, providing a step toward an anatomical chassis for C_4 engineering. Collectively, a conserved mechanism of vein rank specification in grass leaves has been revealed.

INTRODUCTION

Biological patterns form during the development of multicellular organisms, when cell fates are mapped onto fields of equivalent pluripotent cells in organized space and time.[1] In flowering plants, patterning primarily occurs post-embryogenesis at the shoot and root apical meristems, with shoot patterns most obvious in the geometrical arrangement of leaves around the apex and in floral morphologies.[2] Less obvious is the patterning of veins within leaves, which in flowering plants is of two distinct types. In eudicotyledonous (eudicot) plants, leaf veins form reticulated networks, whereas in monocotyledonous (monocot) plants, veins run in parallel along the length of the proximo-distal leaf axis (reviewed in Perico et al.,[3] Roth-Nebelsick et al.,[4] and Sack and Scoffoni[5]). Both patterns are the result of organized specification of vein-forming stem cells (procambial initial cells) within the ground meristem of the leaf,[6] with temporal regulation facilitating the sequential formation of different vein ranks and spatial regulation defining the distance between veins.

Vein patterning mechanisms are best characterized in eudicots, where regulated flux of auxin determines the direction and extent of vein development. In the eudicot *Arabidopsis thaliana* (*Arabidopsis*), auxin flux occurs both via passive diffusion through plasmodesmata[7] and active transport through membrane-localized transporters,[8,9] with the asymmetric distribution of efflux carriers such as PIN FORMED1 (PIN1) directing flux from the leaf margin to the midvein through narrow strands of procambium (reviewed in Scarpella[10]). The specification of procambial initials (referred to as preprocambial cells in *Arabidopsis*[11]) that form the procambial strands occurs when auxin signaling activates expression of the auxin response factor (ARF) *MONOPTEROS/ARF5* (*MP*).[12] MP then elevates PIN1 expression in a feedback loop and induces expression of the HD-ZIP III transcription factor (TF) *ARABIDOPSIS THALIANA HOMEOBOX 8* (*ATHB8*), which marks procambium identity and stabilizes PIN1 localization.[13] The PIN/MP/ATHB8 module thus reinforces auxin flux and leads to the extension of procambial strands. Although procambium develops simultaneously along a file of preprocambial cells, veins form sequentially in rank order, with new procambial strands developing toward, and connecting with, those that have already formed.[14,15]

Mechanisms of vein patterning in monocot leaves appear inherently different from those in eudicots because successive vein ranks are positioned in between and parallel to existing veins, with connections only made late in development when transverse veins form across the medio-lateral leaf axis. Vein ontogeny in monocots is best characterized in grasses such as *Zea mays* (maize), where four longitudinal vein ranks

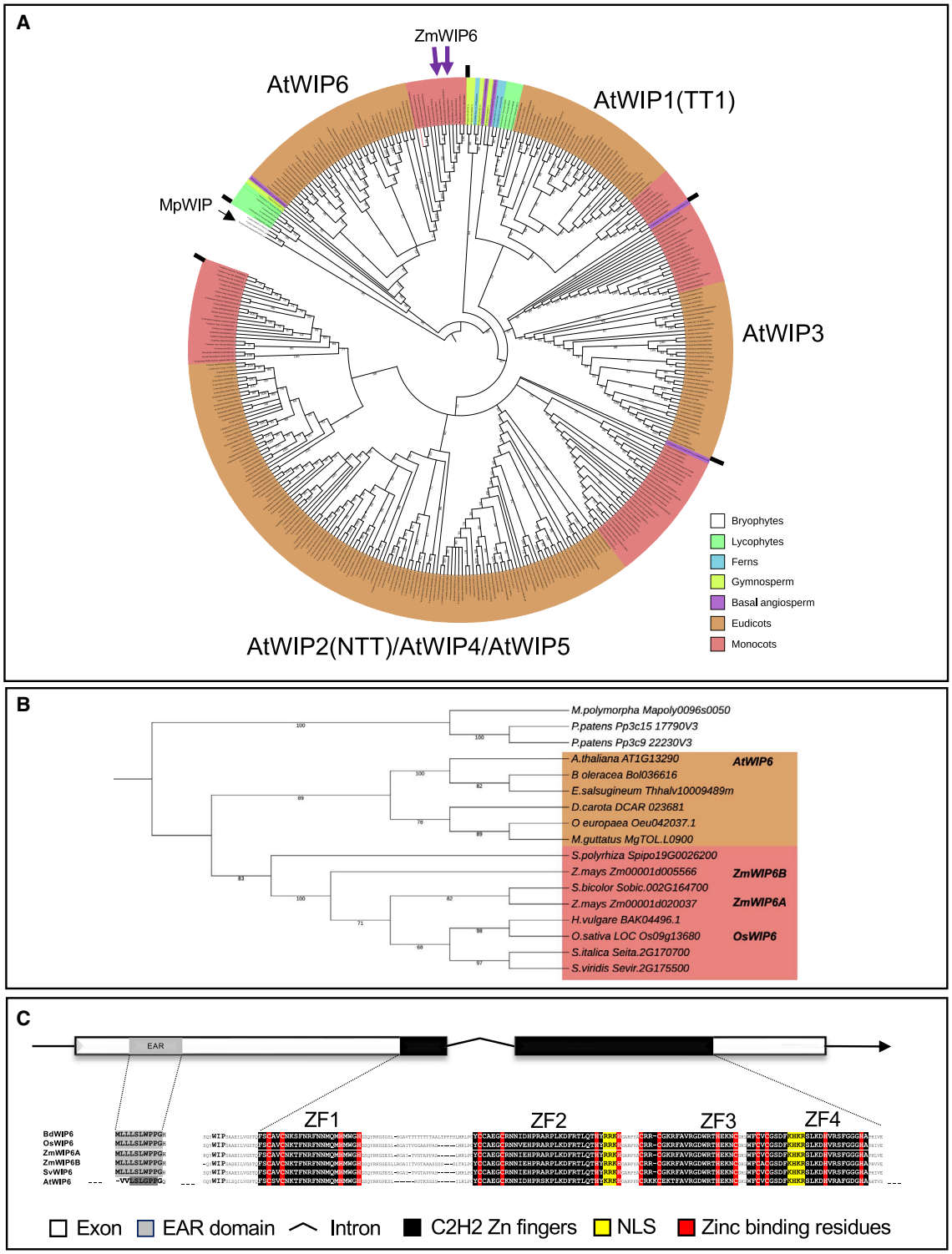

Figure 1. Monocot WIP6 orthologs contain a conserved N-terminal EAR domain

(A) Maximum likelihood phylogeny of WIP proteins in land plants, rooted with the single WIP gene from *Marchantia polymorpha* (*MpWIP*). Six WIP genes are present in *Arabidopsis thaliana*, with four clades identified in basal angiosperms (WIP1, WIP3, WIP2,4,5, and WIP6), and two clades (WIP6 and WIP1-5) identified in all vascular plant lineages. Maize has two genes in the WIP6 clade.

(B) Maximum likelihood phylogeny of WIP6 proteins from representative eudicots (orange shading) and monocots (pink shading), rooted with the bryophyte clade. Bootstrap values are indicated below branches.

(legend continued on next page)

develop.[16,17] The midvein develops first, differentiating from the base of the leaf primordium to the tip, the lateral veins develop next (also toward the tip), and then the rank 1 and rank 2 intermediate veins develop, in turn, from the tip toward the base. Only the largest of the rank 1 veins, which are associated with sclerenchyma on both the adaxial and abaxial sides, extend into the leaf sheath, and veins in the sheath are thus spaced further apart than those in the blade. In maize, the veins underpin a cellular arrangement known as Kranz anatomy in which veins are surrounded by concentric rings of photosynthetic bundle sheath cells and mesophyll cells, and all veins in the blade are separated by just four cells in the medio-lateral leaf axis (reviewed in Sedelnikova et al.[18]). This anatomy, which is associated with C_4 photosynthesis, evolved multiple times from the ancestral anatomy found in C_3 photosynthesizing grasses such as *Oryza sativa* (rice).[19] In C_3 grass leaves, rank 2 intermediate veins are absent and vein pairs are separated by up to ten mesophyll cells. Venation patterns in C_4 leaves therefore differ from C_3, both in terms of the spacing between veins (closer in C_4) and in the number of vein ranks (more in C_4) (reviewed in Perico et al.[3]). In both C_4 and C_3 leaves, however, the timing of vein initiation is similar. The midvein initiates at plastochron (P) 1 (where a plastochron is the interval between primordia initiation at the meristem and P1 is the most recent), laterals at P2/P3, and intermediates between P3 and P5.[16,20,21] In each case, procambial cells are marked by *PIN* gene expression[22–25] as in eudicots, but strands are not directed toward existing veins, suggesting that vein spacing across the medio-lateral leaf axis is pre-patterned within ground meristem cells of the emerging primordium. Except for the homeobox gene *OsHOX1*, which is expressed in procambial cells of developing rice leaves,[26] the identity of genes acting downstream of auxin during the formation and extension of procambial strands in monocot leaves remains elusive.

Here, we identify a gene encoding a WIP C2H2 zinc finger (ZF) protein[27] that is expressed in procambial initial cells in the leaves of multiple grass species. The maize gene Zm00001d020037 (B73 v3—GRMZM2G150011; B73 v5—Zm00001eb309530) was first identified as a candidate regulator of vein patterning in a transcriptome analysis of maize foliar and husk leaf primordia.[28] Transcript accumulation profiles from P1 to P5 indicated an increase in expression levels prior to the initiation of veins in developing P1/P2 primordia and a decrease after P5 once all veins had been specified. The gene was hypothesized to be a regulator of Kranz anatomy.[29] Through loss-of-function analyses in maize and *Setaria viridis*, we demonstrate that the WIP6 gene *TOO MANY LATERALS* (*TML*) facilitates development of the correct ratio of lateral to intermediate veins in C_4 grass leaves. Rather than being specific for Kranz anatomy, however, we show that aspects of TML function are conserved between C_4 and C_3 species, enabling venation patterns to be modified in rice.

RESULTS

A canonical EAR domain is present in monocot but not eudicot WIP6 proteins

To dissect the function of the maize gene Zm00001d020037, orthologous genes were identified in predicted proteomes of all species using Orthofinder[30] (Data S1). The orthogroup contains WIP proteins, which are specific to land plants and are characterized by a conserved three amino acid "WIP" sequence and four ZF domains.[31] Phylogenetic inference revealed a single gene in the bryophyte *Marchantia polymorpha* (*MpWIP*), evidence of a gene duplication that generated WIP6 and a second clade in the last common ancestor of vascular plants, and further duplications in the last common ancestor of flowering plants that subdivided the second clade into WIP1, WIP3, and WIP2/4/5 clades (Figure 1A; Data S2). Zm00001d020037 and its paralog Zm00001d005566 are members of the WIP6 clade. The only gene in this clade for which function has been reported is *Arabidopsis WIP6*, which was named *DEFECTIVELY ORGANISED TRIBUTARIES 5* (*DOT5*) because of leaf venation defects observed in a transposon insertion line.[32] However, recent work refuted a role for *AtWIP6* in venation patterning, being unable to identify any developmental perturbations in loss-of-function mutants created by gene editing.[33,34] In the absence of a known function, we therefore named the maize genes *ZmWIP6A* (Zm00001d020037) and *ZmWIP6B* (Zm00001d005566).

Within the WIP6 clade, eudicot and monocot sequences form two discrete sub-clades (Figures 1A, 1B, and S1A; Data S1 and S2). In the monocot clade, most genomes contain a single WIP6 copy as seen in the basal monocots *Zostera marina* and *Spirodela polyrhiza*. In maize, *ZmWIP6A* (chromosome 7) and *ZmWIP6B* (chromosome 2) are not in syntenic regions of the genome[35] and are thus unlikely to have arisen from the whole-genome duplication event that generated many homeologous genes in the species. A protein alignment of 50 WIP6 protein sequences from 41 species highlights the WIP sequence plus the four highly conserved ZF domains arranged in tandem at the C terminus[27,31,36] (Figures 1C and S1B; Data S1). Toward the N terminus, a putative ethylene-responsive element binding factor-associated amphiphilic repression (EAR) motif (LxLxPP)[37] is present in both eudicot and bryophyte proteins, but only the monocot proteins contain a *bona fide* LxLxL-type EAR motif.[38] Given that LxLxL EAR motifs are known to mediate transcriptional repression of target genes,[37] the observed differences could reflect a repressor role for WIP6 proteins, specifically in monocots.

WIP6 gene transcripts accumulate in procambial cells that will form intermediate veins in grass leaf primordia

Transcripts of both *ZmWIP6A* and *ZmWIP6B* accumulate to relatively low levels in whole-leaf primordia (550 and 80 transcripts per million, respectively[28]), but expression analyses at the whole-tissue level can mask big differences between individual

(C) Schematic representation of monocot WIP6 genes, showing 5′ and 3′ UTRs (black lines) plus two exons (rectangles) separated by an intron (). The arrow indicates the direction of transcription, the conserved EAR domain (gray box) and the C2H2 ZF region (black boxes) are highlighted. The protein alignment illustrates the amino acid residues in the conserved protein domains. The LxLxL-type EAR motif present in monocot WIP6 proteins is not present in eudicot proteins (Figure S1). A WIP domain (in bold) and up to four ZFs are predicted. The ZFs are highlighted in black with the zinc binding residues in red and the nuclear localization signal (NLS) is highlighted in yellow.
Supported by Figure S1 and Data S1 and S2.

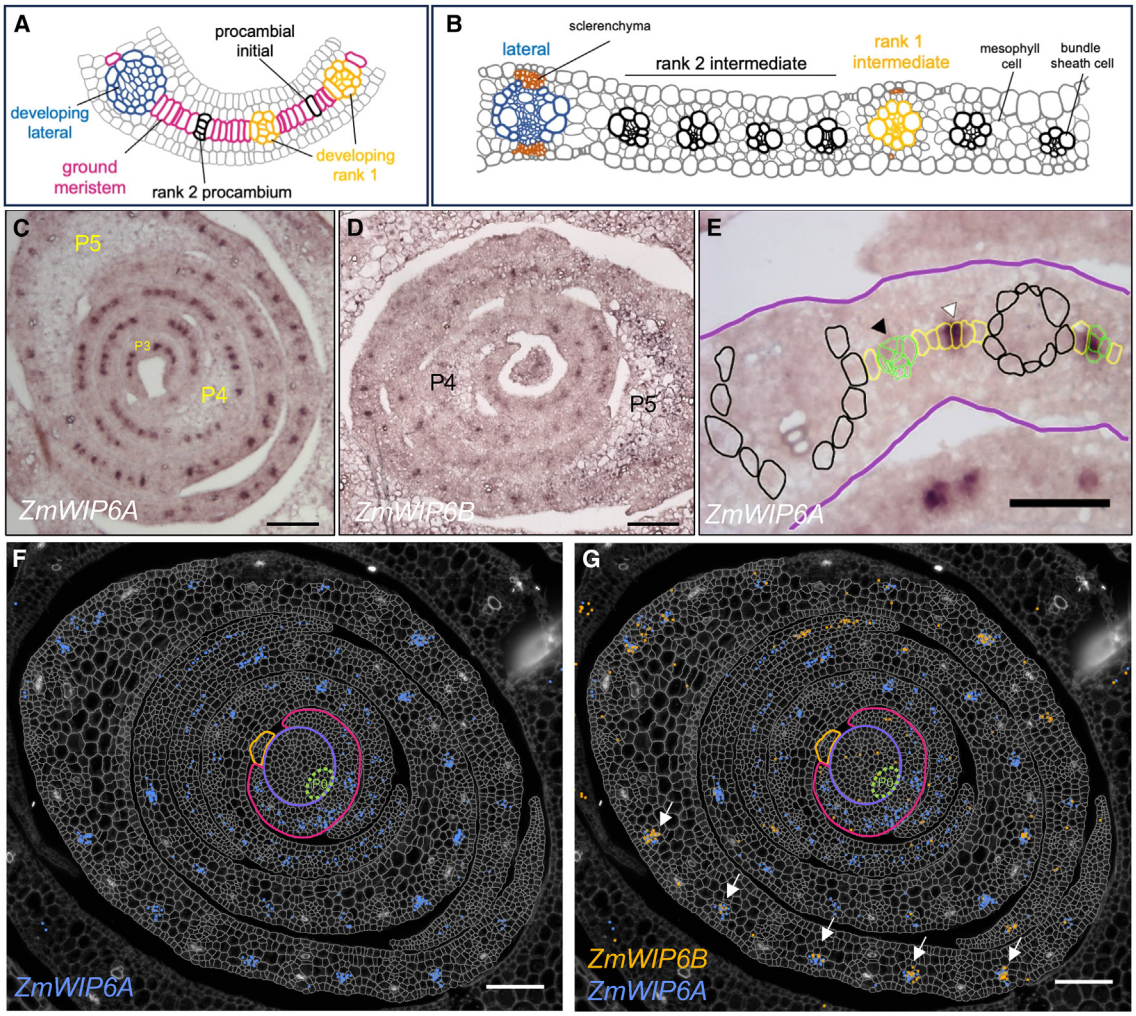

Figure 2. WIP6 genes are expressed in dividing procambial cells in maize leaf primordia

(A and B) Schematics of cellular arrangements in a P4 primordium (A) and an expanded leaf (B). Different vein and cell-types are indicated.

(C and D) *In situ* hybridization of *ZmWIP6A* (Zm00001d020037) (C) and *ZmWIP6B* (Zm00001d005566) (D) transcripts to P3–P5 leaf primordia of maize. Plastochron stages are as indicated. Scale bars, 100 μm.

(E) Annotated image of a section hybridized with *ZmWIP6A*. The P5 primordium is outlined in purple and ground meristem cells are outlined in yellow. Four different stages of vein development are highlighted. The white arrowhead marks a procambial initial, which can only be distinguished from the surrounding ground meristem cells by the presence of *ZmWIP6A* transcripts. The green cells denote early dividing procambial centers, with the black arrowhead marking the more advanced stage. Black cells surround fully differentiated veins. *ZmWIP6A* transcripts are detected in the procambial initial and in the early dividing procambium but are absent once the developing vein comprises more than four or five cells (black arrowhead). Scale bar, 50 μm.

(F and G) Molecular cartography showing accumulation of *ZmWIP6A* (Zm00001d020037) (blue dots in F and G) and *ZmWIP6B* (Zm00001d005566) (orange dots in G) transcripts in the shoot apical meristem and P1–P5 leaf primordia of maize. The purple line indicates the meristem, green dotted line the P0 primordium, orange line the P1 primordium, and pink line the P2 primordium. White arrows indicate developing intermediate veins in the P5 leaf sheath tissue. Scale bar, 100 μm. Supported by Figure S2.

cells. To evaluate the spatial pattern of *ZmWIP6A* and *ZmWIP6B* expression, *in situ* hybridization experiments were performed with sections of maize shoot apices that included P2–P5 leaf primordia. For orientation, Figure 2A illustrates a P4 leaf primordium with procambial initial cells and procambial centers (dividing procambial cells that will give rise to veins), and Figure 2B shows an expanded leaf with lateral and intermediate veins. Transcripts were detected in developing procambial centers of P3, P4, and P5 primordia, with *ZmWIP6A* accumulating to higher levels than *ZmWIP6B* in the leaf blade (as seen in transcriptomic experiments) (Figures 2C and 2D). The presence of veins at different stages of development in each leaf primordium further revealed the temporal pattern of *ZmWIP6* expression, with transcripts present in the single procambial initial cell, and in the first four or five derivatives of that cell during the initiation of intermediate veins, but absent at later stages of development (Figure 2E). Similar spatial expression profiles were seen in other grass species, with expression of the single WIP6 ortholog in each case being confined to developing veins in *Setaria viridis*, *Sorghum bicolor*, and rice primordia

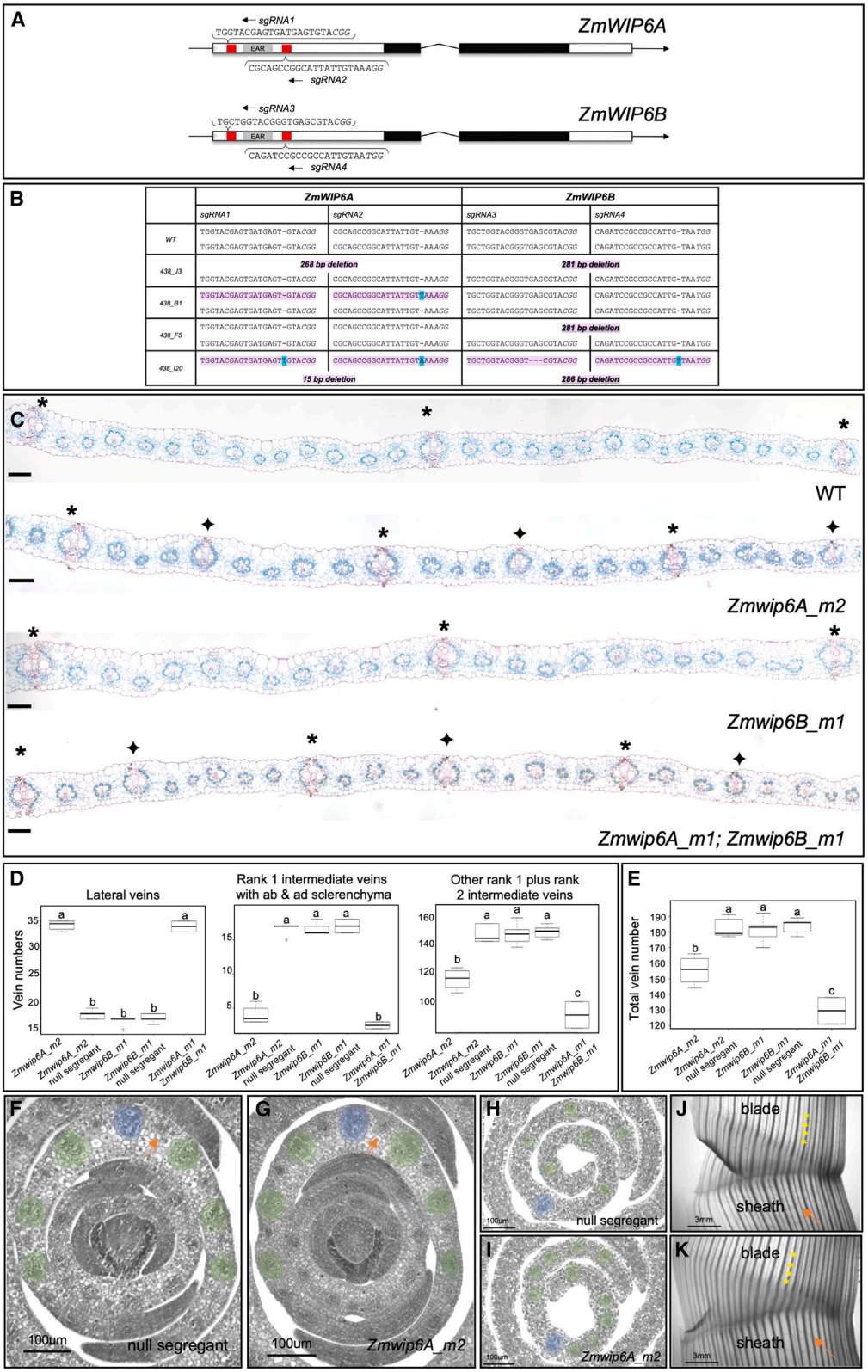

(legend on next page)

(Figures S2A–S2C). In rice, however, where veins are initiated further apart than in the three other species, the temporal profile of *OsWIP6* expression differed in that transcripts were detectable at later stages of vein development than seen in maize (Figure S2D). Collectively, these data suggest that WIP6 orthologs may play a role in the specification of procambial initial cells within the ground meristem of developing leaf primordia in both C_4 and C_3 species.

To gain a better understanding of *ZmWIP6* expression profiles and to examine transcript accumulation patterns in the shoot apical meristem plus P0 and P1 leaf primordia, fragments of both genes were hybridized to maize shoot apices using Resolve Biosciences Molecular Cartography technology. Cellular localization and quantification of both transcripts revealed an overlapping but distinct expression pattern for each gene. Specifically, *ZmWIP6A* is expressed in developing intermediate veins of all leaf primordia examined, whereas *ZmWIP6B* is only expressed in a subset (Figures 2D and 2E). Neither gene is expressed in the midvein or lateral veins at any stage of development. (Note that although some signal was detected in the early P2 primordium where intermediate veins have yet to be initiated, the signal was not localized to procambial centers.) Co-localization of *ZmWIP6A* and *ZmWIP6B* transcripts is most apparent in developing intermediate veins of P5 primordia (arrows in Figures 2E and S2). Because a transverse section across the shoot apex captures leaf primordia at different positions along their proximo-distal axes, the P1 section is at the very tip of the blade, P2 and P3 are near the middle of the blade, P4 is at the base of the blade, and P5 is in the leaf sheath. Given that intermediate vein development in the leaf sheath is the last stage of vein patterning within any grass leaf primordium, these observations suggest that *ZmWIP6A* may function from the earliest stages of intermediate vein formation, whereas *ZmWIP6B* may only be required either late in development or specifically in the leaf sheath. Intriguingly, although *ZmWIP6A* activity appears to be restricted to the first few divisions in procambial centers of P3–P5 primordia, transcripts are also detected alongside *ZmWIP6B* around mature veins in the leaf sheath. These observations suggest that *ZmWIP6A* may have a non-redundant specification role early in development of the leaf blade and a redundant role with *ZmWIP6B* later in the development of the leaf sheath.

Loss-of-function *Zmwip6A* mutants develop too many lateral veins

To determine whether *ZmWIP6A* or *ZmWIP6B* expression patterns reflect a role in leaf venation patterning, loss-of-function alleles were generated by CRISPR-Cas9-mediated gene editing. Two single-guide RNA sequences (sgRNAs) were designed to target each gene at sites flanking the EAR domain (Figure 3A) and all four sgRNAs were assembled into a single construct for transformation into maize inbred line B104. Resultant T0 plants were backcrossed to B104 and four T1 lines representing different combinations of mutant alleles were obtained (Figure 3B). One line contained mutations in *ZmWIP6A*, one in *ZmWIP6B*, and two in both genes. Within the four lines, there were four independent alleles of *ZmWIP6A* and three of *ZmWIP6B*, with one of the double-mutant lines (438_I20) being heteroallelic at both loci. For *ZmWIP6A*, allele *Zmwip6A_m4* (I20_3) encoded an almost full-length protein with just five amino acids deleted upstream of the EAR domain that was likely to be at least partially functional (Figure S3A). No further characterization was carried out with this allele. The remaining three alleles contained a 268-bp deletion (*Zmwip6A_m1* [J3]) or single base pair insertions (*Zmwip6A_m2* [B1_10] and *Zmwip6A_m3* [I20_18]) that resulted in premature stop codons upstream of the ZF domain and thus represented loss-of-function alleles (Figure S3A). Premature stop codons and loss of gene function were also predicted for three alleles of *ZmWIP6B* (*Zmwip6B_m1*—281 bp deletion [J3]), (*Zmwip6B_m2*—286 bp deletion [I20]), and (*Zmwip6B_m3*—3 bp deletion plus single bp insertion [I20]) (Figure S3B). Homozygous mutations that segregated independently from the transgene were identified in progeny of self-pollinated T2 lines and single and double combinations of mutant alleles were fixed for phenotypic characterization.

To assess the impact of loss of ZmWIP6 function, single- and double-mutant plants were grown alongside null segregants. None of the mutants exhibited general growth perturbations (Figures S3C–S3F). In leaves, venation patterns were perturbed in *Zmwip6A* mutants and in double mutants, but not in *Zmwip6B* mutants (Figure 3C). Specifically, *Zmwip6A* and *Zmwip6A;*

Figure 3. Loss of ZmWIP6A function leads to the formation of too many lateral veins in the maize leaf

(A) Gene models of *ZmWIP6A* and *ZmWIP6B*, showing 5′ and 3′ UTRs (black lines) plus two exons (rectangles) separated by an intron (). The arrow indicates the direction of transcription, the conserved EAR domain (gray box), the C2H2 ZF region (black boxes), and the sgRNA target sites (red) are highlighted. The sgRNA sequences used for CRISPR-Cas9-mediated mutagenesis are as shown, with the protospacer adjacent motif (PAM) sequences in italics.

(B) Allelic composition of WT and four T1 maize lines. Mutant alleles are highlighted in pink and base insertions are highlighted in blue. One line (I20) was heteroallelic at both loci, one (J3) was heterozygous at both loci, and the other two were heterozygous at one locus and WT at the other.

(C) Transverse sections of WT and mutant leaves, showing vein numbers and types. In each case samples were taken from the 5th leaf in the region between laterals 2 and 4, with lateral 1 being the closest to the midvein. Asterisks indicate lateral veins, diamonds indicate ectopic lateral veins. Scale bars, 100 μm.

(D and E) Quantification of the number of each vein type (D) and of total vein number (E) across the entire medio-lateral axis of the 5th leaf. "Other rank 1 veins" are those which only have sclerenchyma on the adaxial or abaxial side but not both. n = 5 for *Zmwip6B_m1*, *Zmwip6A_m2* null segregant, and *Zmwip6B_m1* null segregant, n = 4 for *Zmwip6A_m2*, and n = 2 for the double homozygous *Zmwip6A_m1/Zmwip6B_m1* mutant. Statistical significance was determined using a one-way ANOVA followed by a Tukey's test; see Data S5A for raw data.

(F–I) Transverse sections of null segregant (F and H) and *Zmwip6A_m2* mutant (G and I), P4 primordia at the base (F and G) and in the middle (H and I) of the primordium. Midveins are highlighted in blue and lateral veins (both normal and ectopic) are highlighted in green. Orange arrows point to developing intermediate veins. Scale bars, 100 μm.

(J and K) Cleared fragments of leaf 7 stained with safranin, showing the junction of leaf sheath and blade in null segregant (J) and *Zmwip6A_m2* (K) mutant leaves. Orange arrows point to a rank 1 intermediate, with abaxial and adaxial sclerenchyma in (J) and an ectopic lateral in the equivalent position in (K). Yellow asterisks are positioned at transverse veins. Scale bar, 3 mm.

Supported by Figure S3 and Data S5A.

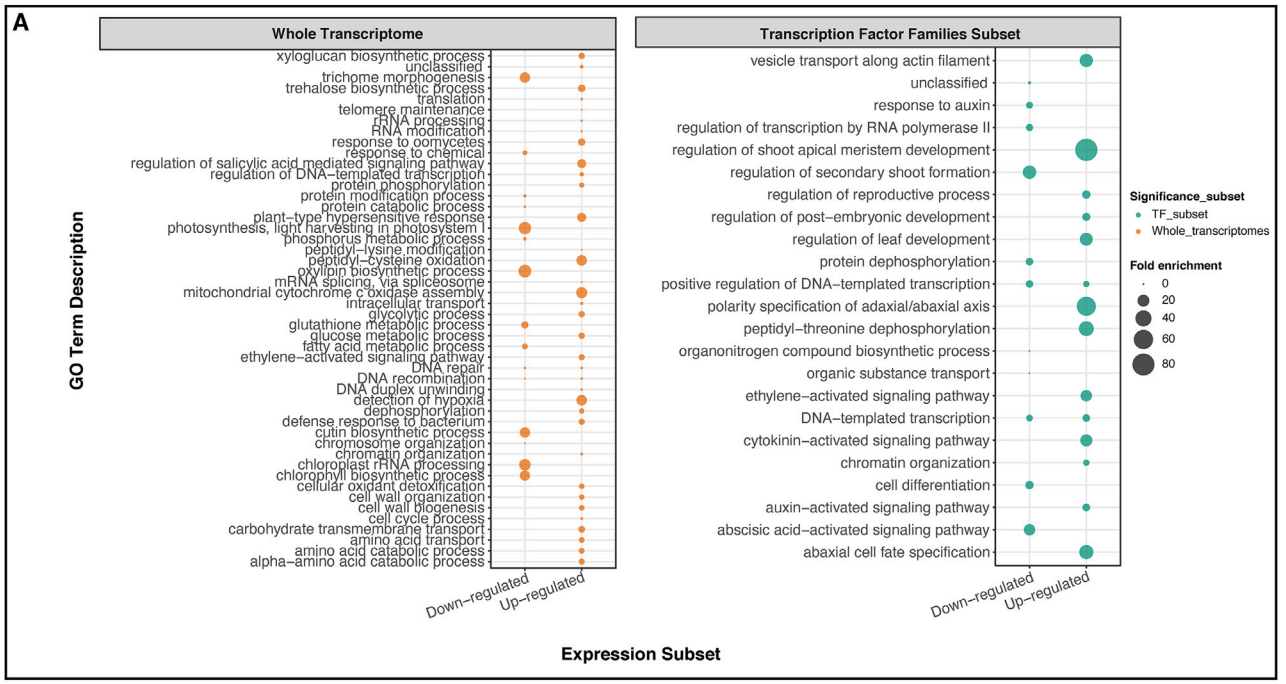

(legend on next page)

Zmwip6B mutant leaves developed twice as many lateral veins than corresponding wild-type (WT) siblings, with a concomitant decrease in the number of intermediate veins (predominantly rank 1 intermediates) (Figure 3D). Notably, the same phenotype was observed in *S. viridis* when the single *SvWIP6* gene was edited (Figures S3C–S3F). Because the number of ectopic lateral veins was the same in single *Zmwip6A* mutants as in double mutants, no role could be inferred for *ZmWIP6B* in the regulation of vein type. When total vein number across the medio-lateral axis was quantified, however, *Zmwip6B* mutants were indistinguishable from WT, whereas the two double mutants that were analyzed had fewer veins than *Zmwip6A* mutants (Figure 3E). We thus conclude that *ZmWIP6B* plays a minor (yet unidentified) role in venation patterning compared with *ZmWIP6A*. Based on the mutant phenotypes, we renamed *ZmWIP6A* and *ZmWIP6B* genes TML (*ZmTML1* and *ZmTML2*) and, because of the conserved mutant phenotype, the *S. viridis* ortholog was named *SvTML*.

Extra lateral veins in *Zmtml1* mutants could result from the specification of additional lateral veins or from mis-specification of intermediate veins. To distinguish these possibilities, transverse sections were examined at the base and middle of P4 primordia (Figures 3F–3I). If extra lateral veins result from ectopic specification, more laterals would be visible at the base of mutant primordia than in null segregants because lateral veins differentiate from base to tip and are specified by P4. By contrast, if the phenotype results from mis-specification of intermediate veins, developing veins positioned between lateral veins in the middle of mutant primordia would be larger (more lateral-like) than in null segregants because intermediate veins develop from tip to base and at P4 they are more differentiated in the middle than at the base of the leaf. Figures 3F and 3G show that the number of lateral veins at the base of the P4 primordium is the same in null segregant and mutant samples. Developing veins positioned between the laterals look slightly larger in the mutant than in the null segregant, but in both cases they are smaller than adjacent lateral veins. Comparisons between Figures 3H and 3I, however, reveal more veins with lateral identity in the middle of mutant primordia than in null segregants. Because ectopic lateral vein identity is evident in the middle but not the base of the primordium, we conclude that the mutant phenotype arises from mis-specification of basipetally differentiating intermediate veins as lateral veins. This conclusion is validated because the rank 1 intermediate veins that extend into the sheath are clearly distinguishable from adjacent lateral veins in null segregants, but in mutant leaves they are not (Figures 3J and 3K). Notably, these longitudinal images also revealed no differences between mutants and null segregants in the pattern of transverse veins connecting lateral and intermediate veins across the medio-lateral leaf axis (Figures 3J and 3K). During WT development, *ZmTML1* must therefore act to suppress lateral vein identity in procambial centers that form rank 1 intermediate veins, specifically those rank 1 veins that are associated with sclerenchyma on both the adaxial and abaxial sides and extend from the leaf blade into the leaf sheath.

Transcriptomes suggest altered cell division dynamics and auxin responses in *Zmtml1tml2* mutants

To identify potential targets of *ZmTML* function during early leaf development and to assess which processes are perturbed in mutant leaves, transcriptome profiles were compared between shoot apices (composed of the shoot apical meristem and P1–P5 leaf primordia) of double *Zmtml1tml2* mutants and segregating WT siblings. Transcripts were quantified to identify those where levels showed a significant difference ($\log_2$ fold change [L2FC] > 1; $p < 0.05$) between WT and mutant (Data S3A). (All fold differences referred to below are L2FC at $p < 0.05$.) Levels of transcripts encoded by 591 genes were significantly higher in mutant samples than WT and those encoded by 1,275 genes were lower. Gene Ontology (GO) term enrichment analysis revealed a broad range of functions that are perturbed in mutant plants, with those encoding TFs notably enriched for terms associated with shoot apical meristem development and adaxial/abaxial axis specification (Figure 4A). 89 transcripts representing 47 genes were up-regulated greater than 20-fold in the mutant, with the majority encoding enzymes or structural proteins (Data S3A). By contrast, 45 transcripts representing 24 genes were down-regulated greater than 20-fold in the mutant and, of the 11 genes in that group that have been annotated, 5 encode proteins that regulate gene activity (Data S3A).

Of the few genes directly implicated in the development of Kranz anatomy (*SHORTROOT* [*SHR*],[39] *SCARECROW* [*SCR and SCR1h*],[40–42] and *NAKED ENDOSPERM* [*NKD1* and *NKD2*],[43] only *NKD2* transcript levels were significantly different between mutant and WT (lower in the mutant—L2FC = 1; $p < 0.05$) (Data S3B), suggesting that *ZmTML* genes act downstream of any "Kranz patterning module." Notably, the failure to detect differences in levels of transcripts encoding orthologs of procambial markers in *Arabidopsis* (*ATHB8*/*ZmHB52* and *PIN1*) and rice (*OsHOX1*/*ZmHB78*) (Data S3B) could also suggest that ZmTML function is downstream of procambium initial cell specification. The development of normal vein numbers in loss-of-function *Zmtml1tml2* mutants (Figures 3D and 3E) would also support this suggestion. However, *ZmHB52* is expressed more broadly than *ZmTML1* in WT leaf primordia, with transcripts detected across the P1 leaf primordium and in the more actively dividing cells at the margins of older primordia (Figures S4A and S4B). Restriction of *ZmHB52* transcripts to dividing procambial centers only occurs after *ZmTML1* transcript accumulation is repressed in those regions. We therefore propose that *ZmTML1* acts downstream of mechanisms that spatially regulate where veins are initiated, acts earlier than *ZmHB52* in vein

Figure 4. Evidence of auxin and CK pathway perturbations in *Zmtml1tml2* mutant transcriptomes

(A) Overrepresentation analysis (ORA) of significantly different transcript levels (L2FC > 1; $p \leq 0.05$) in *Zmtml1tml2* mutant apices as compared with corresponding segregating WT siblings, using data either from the whole transcriptome or from the subset annotated as TFs. Down- and up-regulated components are as indicated and the fold-enrichment in each case is shown by the size of the bubble.

(B) $\log_2$ fold difference in levels of transcript encoding auxin and CK pathway components in *Zmtml1tml2* mutant apices as compared with corresponding segregating WT siblings. For each pathway step, the genes with significantly different transcript levels (L2FC ± 1; $p \leq 0.05$) are labeled.

Supported by Figure S4 and Data S3.

development, and that any role in specifying procambial initial cells is carried out redundantly with other (yet unidentified) partners such that procambium is positioned in the correct locations in mutant leaves.

Of the 529 differentially expressed TF encoding genes (L2FC > 1; $p < 0.05$), greater than 4-fold differences in transcript levels between WT and mutant were observed for members of 24 different TF families (Figure S4C). 20-fold higher levels of *ZmGRF1* (*GROWTH REGULATING FACTOR 1*) transcripts in mutants than in WT segregants were particularly notable because *ZmGRF1* transcript levels are normally tightly regulated post-transcriptionally by miR396a.[44] What is more, constitutive overexpression of a miRNA-resistant version of *ZmGRF1* in maize was associated with a larger cell division zone at the base of developing leaves, with increased numbers of normal sized cells dividing more slowly than in WT counterparts.[45] Upregulation of *ZmANT1* (*ZmEREB184*) (L2FC > 6; $p < 0.05$) in mutants (Figure S4C) is also notable because of a proposed role in cell proliferation during leaf development.[46] The phenotype of *Zmtml1tml2* mutant leaves may thus be caused in part by altered cell division dynamics in developing leaf primordia and *ZmGRF1* and/or *ZmANT1* expression may be directly or indirectly repressed by ZmTML1 and/or ZmTML2.

Because the spatial and temporal extent of cell division zones within developing grass leaves has been associated with the regulation of cytokinin (CK) signaling (higher levels are present in the division zone),[47,48] and GO-terms associated with CK were enriched in the population of differentially expressed genes (Figure 4A), we next sought to determine which components of the CK pathway were perturbed in *Zmtml1tml2* mutants. To this end, we compiled a list of genes involved in CK biosynthesis, signaling, degradation, and response (Data S3C), and quantified transcript levels for each. Of the 150 genes analyzed, 11 exhibited significant differences between WT and mutant (Figure 4B; Data S3D). The most substantial differences were seen for transcripts encoding two histidine kinase CK receptors (decreased in the mutant by more than 9-fold [*ZmHK1/HSF1*[49]] and 7-fold [*ZmHK5*]), a homolog of the CK efflux transporter ABCG14 in *Arabidopsis*[50] (reduced more than 7-fold in the mutant) and the CK-oxidase-degrading enzyme ZmCKX11[51] (increased more than 4-fold in the mutant). Collectively, these observations suggest that overall CK activity is repressed in *Zmtml1tml2* mutant apices and thus that cell division dynamics may be perturbed in the shoot apical meristem and/or leaf primordia.

Given that a role for auxin in leaf venation patterning is well established, we predicted that components of the auxin pathway would also be perturbed in *Zmtml1tml2* mutants. Indeed, significant differences were observed in levels of transcripts encoding several ARFs that bind directly to the promoters of auxin responsive genes (reviewed in Lavy and Estelle[52]) (Figure S4C). To determine the point(s) at which perturbations in the auxin pathway were manifest, we compiled a list of genes involved in auxin biosynthesis, conjugation, transport, signaling, and response and quantified transcript levels for each (Data S3E). Of the 186 genes analyzed, 31 exhibited significant differences between mutant and WT (Figure 4B; Data S3F). Although all steps of the pathway showed some perturbation, biosynthesis, and transport steps were least impacted, suggesting that these are upstream of TML function. Except for *ALDEHYDE OXIDASE1* (*ZmAO1*), where transcript levels were elevated over 20-fold in the mutant, the most substantial differences in transcript levels were seen for genes encoding components involved in auxin signaling. Aldehyde oxidases have been implicated in the synthesis of tryptophan precursors for indole-3-acetic acid (IAA) biosynthesis.[53] However, direct functional analyses are lacking, and given that there is no evidence that downstream components of the auxin biosynthesis pathway are similarly elevated, we cannot speculate on the significance of any potential increase in tryptophan levels. Of the signaling components: *ZmSAR1*, *ZmARF4*, and *ZmARF3* were down-regulated more than 7-fold in the mutants; *ZmARF39/ZmABI17*, *ZmARF36*, and *ZmARF13* were up-regulated more than 7-fold; and *ZmARF30* and *ZmARF16* were up-regulated more than 4-fold. Note that *ZmARF4* is a co-ortholog (with *ZmARF29*) of *MP* in *Arabidopsis*, mutations in which reduce the complexity of leaf venation patterns and disrupt axis formation in the embryo.[54,55] *ZmSAR1* encodes the ortholog of *Arabidopsis* SUPPRESSOR OF AUXIN RESISTANCE 1, which is a nucleoporin that facilitates nuclear localization of AUX/IAA proteins.[56] Reduced *ZmSAR1* transcript levels may thus suggest that the ability of AUX/IAA proteins to bind and repress ARFs is compromised in *Zmtml1tml2* mutants, which would translate into increased activation of ARF proteins. Notably, the three most highly up-regulated *ARF* genes in *Zmtml1tml2* mutants are class B repressors and the two down-regulated *ARF* genes are class A activators.[57] The loss of ZmTML function may thus lead to an overall repression of auxin responses, but the possibility that responses are differentially up- or down-regulated in different spatial domains of the shoot apex cannot be discounted.

Transgenic lines that constitutively express *ZmTML1* in rice could not be isolated

With the finding that *ZmTML1* represses lateral vein formation, we hypothesized that ectopic expression in rice would increase intermediate vein number in the leaf. Given that a higher proportion of intermediate veins is a key trait of C_4 leaves, and an engineering goal is to make rice leaves more C_4-like,[58,59] we first tried to constitutively express *ZmTML1* in rice. Constructs in which expression of the maize *TML1* coding region was driven by the constitutive maize ubiquitin promoter (Figure S5A) were transformed on multiple occasions (n = 7) and callus was propagated to the greening stage on selection medium. However, shoots could not be regenerated. This observation suggested that *ZmTML1* may suppress all vein formation and/or the pluripotency required for shoot regeneration.

TML promoter activity is suppressed in transgenic rice lines

The failure to regenerate rice callus that constitutively expressed the *ZmTML1* gene from maize led us to consider that gene dosage and/or expression levels may need to be tightly regulated (spatially and/or temporally). To generate a chassis in which we could test this hypothesis, we edited the *OsTML* (*OsWIP6*) gene (LOC_Os09g13680) that encodes a protein with 71.4% amino acid identity to *ZmTML1*. Edited alleles were generated either using a sgRNA1 designed to target between the EAR and ZF domains or by using sgRNA1 along with two

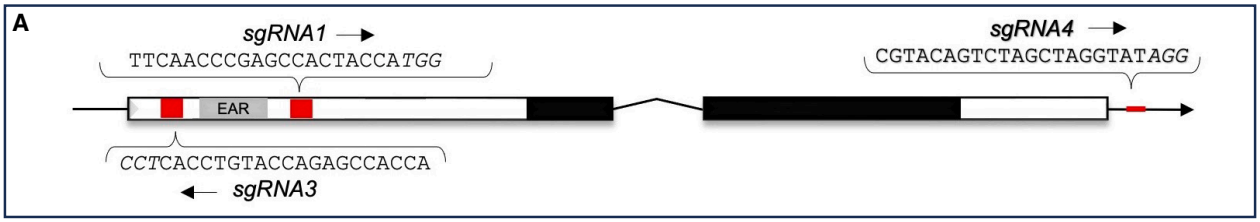

B

	sgRNA1	sgRNA3	sgRNA4
WT	TTCAACCCGAGCCACTA--CCA**TGG**	**CCT**CACC-TGTACCAGAGCCACCA	CGTACAGTCTAGCTAGG-TAT**AGG**
Osdot1_m1	TTCAACCCGAGCCACTAAACCA**TGG**	**CCT**CACC-TGTACCAGAGCCACCA	CGTACAGTCTAGCTAGG-TAT**AGG**
Osdot1_m2	TTCAACCCGAGC-------CCA**TGG**	**CCT**CACC-TGTACCAGAGCCACCA	CGTACAGTCTAGCTAGG-TAT**AGG**
Osdot1_m3.1	TTCAACCCGAGCCACTA--CCA**TGG**	**CCT**CAC--TGTACCAGAGCCACCA	CGTACAGTCTAGCTAGG-TAT**AGG**
Osdot1_m3.3	TTCAACCCGAGCCACTA--CCA**TGG**	**CCT**CAC--TGTACCAGAGCCACCA	CGTACAGTCTAGCTAGGTTAT**AGG**
Osdot1_m4	TTCAACCCGAGC-------CCA**TGG**	**CCT**CACCTGTACCAGAGCCACCA	CGTACAGTCTAGC-------T**AGG**

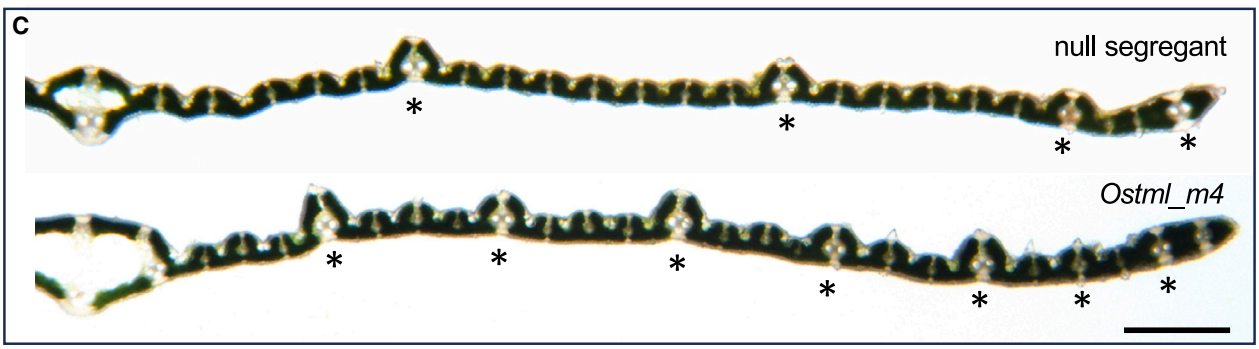

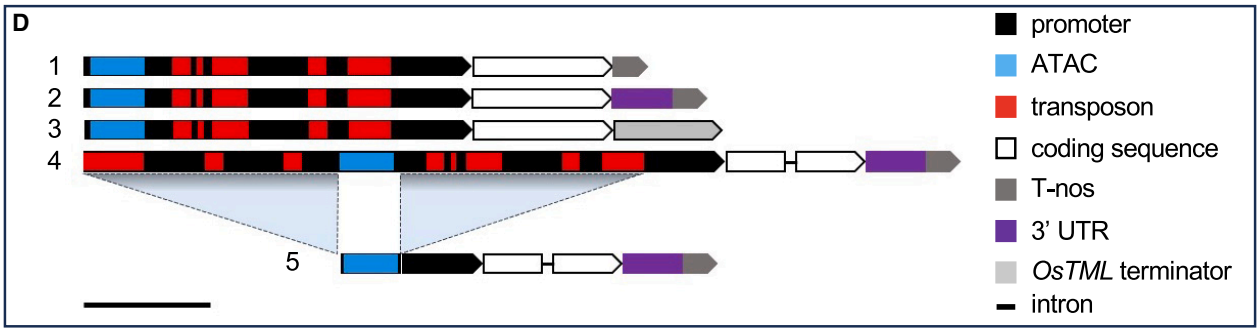

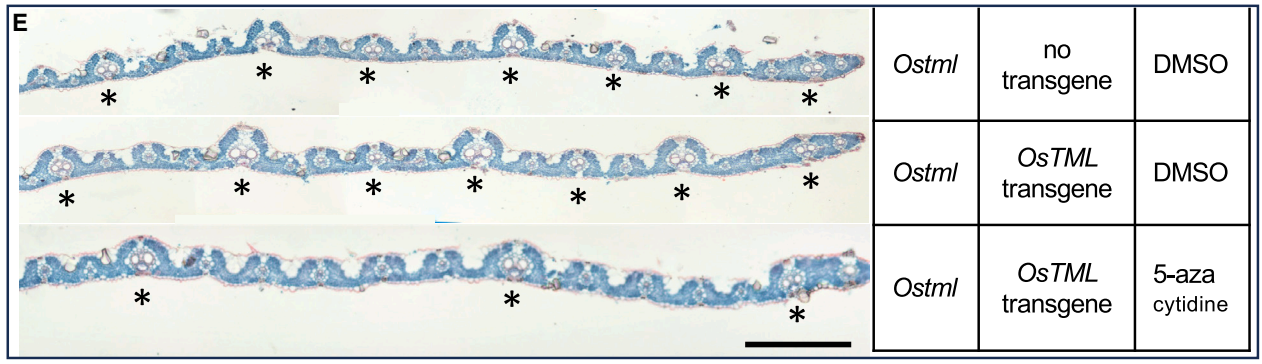

Ostml	no transgene	DMSO
Ostml	*OsTML* transgene	DMSO
Ostml	*OsTML* transgene	5-aza cytidine

(legend on next page)

additional guides (sgRNA3 and sgRNA4) that targeted the 5′ and 3′ regions of the coding sequence, respectively (Figure 5A). Five loss-of-function alleles isolated from the two independent transformation experiments contained short indels at single or multiple guides, resulting in aberrant or truncated proteins (Figure 5B). Mutations were either homozygous or heteroallelic at TO. After backcrossing to WT, F1 plants were self-pollinated and F2 populations segregated mutant progeny as a recessive trait. Notably, all plants carrying loss-of-function alleles showed an increased proportion of larger, lateral-like veins in the leaf blade (Figure 5C), suggesting that *TML* gene function is conserved in maize and rice.

The similar phenotypes of *Zmtml1* and *Ostml* mutants suggested that any TML-mediated difference in venation patterns between the two species must result from different domains of activity in the leaf. We thus revisited the question of whether maize-type expression patterns could alter venation patterns in rice and transformed the *ZmTML1* gene under the control of its own promoter (Figure S5B; Data S4) into the *Ostml* mutant and WT Kitaake rice. Five hygromycin-resistant transgenic lines were obtained in the *Ostml_m1* background and 24 lines in the WT background, but no phenotypic changes were detected in any of the lines tested. This observation suggested either that the *ZmTML1* gene had recombined out of the transgene construct, that the *ZmTML1* promoter sequence did not contain essential regulatory regions, or that transgene expression was suppressed.

Given that we were unable to obtain transgenic lines that expressed *ZmTML* from either a constitutive promoter or from its own promoter, we tested whether endogenous *OsTML* expression patterns could be faithfully reproduced in a series of complementation experiments. First, a 2,945-bp promoter sequence located directly upstream of the start codon and containing a regulatory region predicted by assay for transposase-accessible chromatin with sequencing (ATAC-seq) was fused to the *OsTML* coding sequence and to either the *nos* terminator (construct 1), the *nos* terminator plus 458 bp of the *OsTML* 3′ UTR that contained an 83-bp element conserved in rice, maize and setaria (construct 2), or ~1 kb of the *OsTML* sequence downstream of the stop codon (construct 3) (Figure 5D). The three constructs were individually transformed into WT and *Ostml_m1* (construct 1) or *Ostml_m2* and *Ostml_m3.1* (constructs 2 and 3) lines. In each case, transgenic plants were successfully regenerated but no complementation was observed (see examples in Figures S5C and S5D). As with *ZmTML1*, therefore, the transgenic rice promoter sequence was either lacking essential elements or expression was suppressed. To distinguish these possibilities, two further constructs were tested (Figure 5D). One contained the *OsTML* genomic region, comprising 5.35 kb of upstream sequence, both exons and the intron, plus 458 bp of downstream sequence (construct 4). Because the upstream genomic region contained multiple transposon sequences that may induce host silencing responses, these were removed in the second construct, leaving the ATAC sequence fused directly to the proximal promoter (construct 5). Both constructs were transformed into the *Ostml_m3.1* background but neither complemented the mutant phenotype (Figures S5C and S5D). Although still formally possible that essential elements were missing from the genomic constructs, this observation suggested that transgene expression was being suppressed, even in the absence of transposon sequences within the promoter. To test this hypothesis, seed from lines containing construct 2 were germinated on 50 mg/L 5-azacytidine to demethylate the genome. Although pleiotropic, this treatment led to complementation of the *Ostml* mutant phenotype, presumably by activating *OsTML* transgene expression (Figure 5E). Collectively, these observations suggest that *TML* gene expression is tightly regulated *in planta* and that any mis-expression (spatial and/or temporal) induced via transgenesis is likely to be suppressed or to cause developmental arrest.

Loss-of-function mutations in *OsTML* specifically alter venation patterns in the leaf

Given the inability to modify *TML* expression patterns in rice, we characterized venation patterns in loss-of-function *Ostml* mutants. In terms of overall morphology, the mutant lines did not differ substantially from null segregants (Figure 6A), although *Ostml-m3.1* plants were shorter than WT (Figure S6A). There were no apparent vascular defects in the roots, rachis, or pedicel of mutant plants (Figures S6B–S6D), but venation defects in the leaf were apparent as early as P3, where veins developing in the position of intermediate veins were visibly larger in mutants than in corresponding WT (Figures S6E and S6F). Significantly more lateral veins (Figures 6B and 6C) and fewer intermediate veins (Figure 6D) were observed in leaves of all mutant lines, but there was no change in vein density (Figure 6E). Importantly, the alterations to vein patterning were accompanied by altered bundle sheath cell occupancy in the leaf. In WT rice, bundle sheath cells are rectangular when viewed paradermally, with the long edges running parallel to the vein and the short edges aligned with the medio-lateral leaf axis (Figure 6F). The length of individual bundle sheath cells around veins is highly variable but quantification revealed no significant differences between cell length around lateral versus intermediate veins in WT, *Ostml_m3.1* or *Ostml_m3.3* mutant samples (Figure 6G). The one exception was seen in *Ostml_m4* mutants, where cells around both lateral

Figure 5. Ectopic lateral vein formation in *Ostml* mutants of rice cannot be complemented by *OsTML* because transgene expression is suppressed

(A) Gene model of *OsTML*, showing 5′ and 3′ UTRs (black lines) plus two exons (rectangles) separated by an intron (). The arrow indicates the direction of transcription, the conserved EAR domain (gray box), the C2H2 ZF region (black boxes), and the sgRNA target sites (red) are highlighted. The sgRNA sequences used for CRISPR-Cas9-mediated mutagenesis are as shown, with the PAM sequences in italics.

(B) Allelic composition of WT and five mutant rice lines. Base insertions are highlighted in red.

(C) Transverse sections of null segregant and *Ostml_m4* mutant leaves (flag leaf minus 1). Asterisks indicate lateral veins. Scale bar, 700 μm.

(D) Schematics of 5 transgenes used to complement *Ostml* mutants. Scale bars, ~1 kb.

(E) Transverse sections of leaf 7 from *Ostml_m3.1* mutant lines that were transformed with construct 2 from (D) and were germinated in the presence or absence of 50 mgL^{-1} 5 azacytidine. Asterisks indicate lateral veins. Scale bar, 300 μm.

Supported by Figure S5.

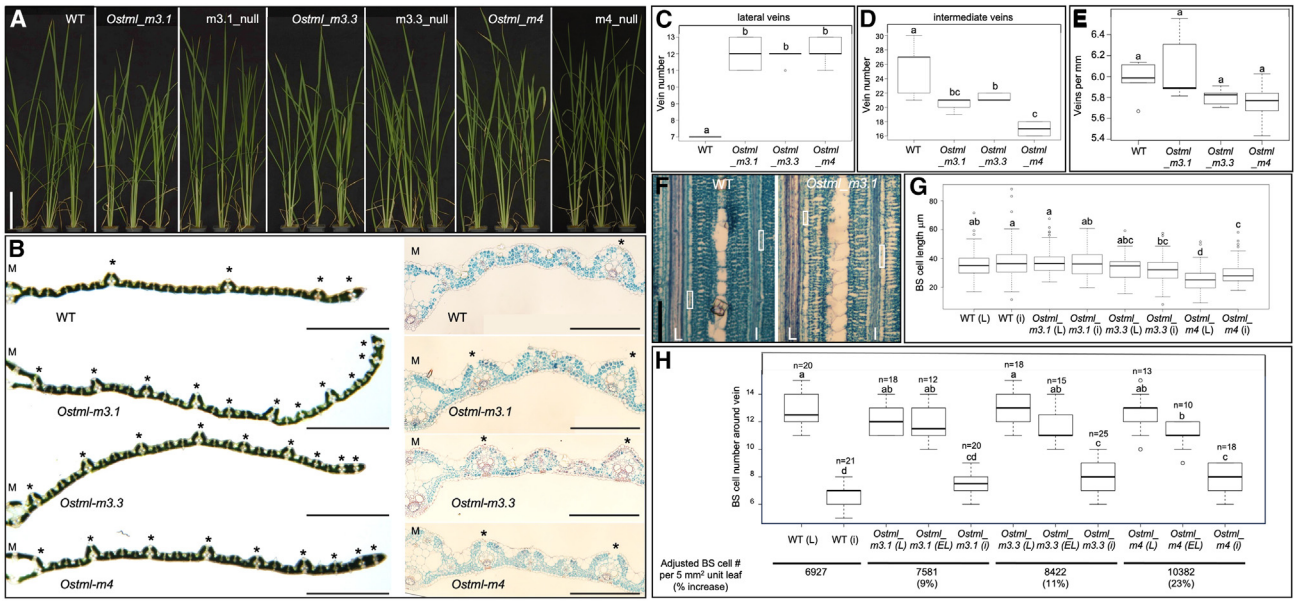

Figure 6. Venation defects in *Ostml* mutant leaves increase total vascular volume and alter bundle sheath cell dimensions

(A) Whole plant phenotype of three independent *Ostml* mutant lines and respective null segregant siblings. Lines were selected from F2 populations that had been generated by backcrossing (BC) transgene free T1 mutants to Kitaake WT and then self-pollinating the resultant BCF1 progeny. Scale bar, 10 cm.

(B) Transverse sections imaged between the midvein and the leaf margin of flag leaf minus 1 (left) and from the midvein to the position corresponding to the first adjacent lateral vein in WT of leaf 4 (right). Asterisks indicate lateral veins. Scale bars, 1 mm (left); 200 μm (right).

(C–E) Quantification of lateral vein numbers (C), intermediate vein numbers (D), and vein density (E) in leaf 7 of WT and mutant plants. n = 5 for each genotype; different letters indicate statistically different groups as determined using a one-way ANOVA followed by a Tukey's test ($p \leq 0.05$); see Data S5B for raw data.

(F) Paradermal images of the 7th leaf of WT and mutant plants, imaged in the middle of the blade. Lateral (L) and intermediate (i) veins are indicated. The longest bundle sheath cell around each vein in the field of view is outlined by a white box. Scale bar, 100 μm.

(G) Quantification of bundle sheath cell length around lateral (including ectopic laterals) and intermediate veins of WT and mutant leaves. n = 4 leaf samples and 82/145 cells around L/i veins for WT; 3 leaf samples and 96/114, 45/44, and 130/130 cells for *Ostml_m3.1*, *_m3,3*, and *_m4* mutants, respectively. Different letters indicate statistically different groups as determined using a one-way ANOVA followed by a Tukey's test ($p \leq 0.05$); see Data S5B for raw data.

(H) Quantification of bundle sheath cells numbers around lateral (L), ectopic lateral (EL), and intermediate (i) veins in WT and mutant plants. Different letters indicate statistically different groups as determined using a one-way ANOVA followed by a Tukey's test ($p \leq 0.05$); see Data S5 for raw data. Median values for bundle sheath length, number of bundle sheath cells, and total vein numbers per leaf were used to estimate total number of bundle sheath cells and percentage increase in number in a leaf unit of 5 mm wide and 1 mm long.

Supported by Figure S6 and Data S5.

and intermediate veins were significantly shorter than those in WT (Figure 6G). When viewed transversely, total bundle sheath cell number across the medio-lateral leaf axis is higher in mutants compared with WT (Figures 6B and 6H) because of the increased proportion of lateral veins in mutant leaves. When the altered cell number across the medio-lateral axis is adjusted to account for variations in cell length along the proximo-distal axis, bundle sheath cell number per unit area is 9%–23% higher in mutant than WT leaves (Figure 6H). Collectively, these observations suggest that vein occupancy in *Ostml* mutant leaves is increased and that there is a substantial increase in the number of bundle sheath cells.

DISCUSSION

Through loss-of-function analyses in three monocot species, we have identified a conserved role for WIP6 orthologs in the specification of vein rank in developing grass leaf primordia (Figures 3, 5, 6, and S3). WIP6 orthologs have been identified in the genomes of all vascular plant groups, as have members of the sister WIP1-5 clade, but just a single *WIP* gene is present in the non-vascular bryophyte *Marchantia polymorpha*[60] (Figure 1). The finding that *MpWIP* is required for the development of air pore complexes on the dorsal surface of the thallus suggests that WIP gene function was initially required for the differentiation of multicellular structures.[60] This is consistent with the observation that members of the WIP1-5 clade in *Arabidopsis* have been shown to play a role in the development of transmitting tract tissue in the pistil (WIP2),[61] the seed coat (WIP1),[31] and the root (WIP2/4/5),[62] specifically in the regulation of cell division orientation in stem cells and cell-type specification. However, original reports of leaf venation defects in loss-of-function *Arabidopsis wip6* mutants[32] were later invalidated,[34] and the suggestion of a non-cell-autonomous role in maternal tissue to suppress cell-type specification in embryonic roots was only inferred from the phenotype of triple *wip1/3/6* mutants.[33] To our knowledge, there are no reports of phenotypic perturbations in single *wip6* loss-of-function mutants in any eudicot.

Based on the conserved phenotype observed in loss-of-function *wip6* mutants in maize, *S. viridis* and rice, we named WIP6 orthologs *TML*. The spatial expression of *TML* genes in procambial initial cells, the temporal restriction of expression to the first

few divisions of those cells and the mis-specification of intermediate veins as laterals in mutant leaves (Figures 2, 3, 5, 6, and S2–S4) are all consistent with a role in cell-type specification and/or divisions of procambial cells in the leaf. The mutant phenotype is also consistent with the role inferred from triple *wip1/3/6* mutants in *Arabidopsis*, namely that of a suppressor.[33] A repressor role is further supported by the observation that constitutive expression of *AtWIP6* conditions a small leaf phenotype in *Arabidopsis*.[63] Notably, general repression of organ growth by WIP proteins has also been demonstrated in melon, where the WIP1 ortholog *CmWIP1* regulates sex determination by repressing carpel primordia in male flowers,[64] and in *Gerbera hybrida*, where overexpression of the WIP2 ortholog suppresses growth in multiple organs.[65] This general repressive role likely explains the failure to regenerate rice callus after transformation with a construct that constitutively expressed *ZmTML1* (Figure S5). It could also explain why attempts to express *TML* genes in rice from the corresponding maize or rice promoters led to transgene silencing (Figure 5). Possibly, the repressive function of TML is only tolerated in the first few divisions of leaf procambial cells and, as such, any leaky expression in callus is silenced. Considering these factors, we propose that TML functions in grass leaves to suppress cell divisions and/or cell fate decisions in procambial cells that lead to the formation of lateral veins, consequently enabling intermediate veins to develop.

The role of TML as a suppressor of lateral vein formation as opposed to an activator of intermediate vein formation is intriguing, not least because it only functions in a subset of the rank 1 intermediate veins. All intermediate veins differentiate from the tip of the leaf primordium toward the base, but only the largest and first to initiate extend into the leaf sheath.[17,18] It is these large intermediate veins that are converted to laterals in *tml* mutants of both maize and rice. The rank 1 intermediate veins that only differentiate sclerenchyma on the abaxial or adaxial side and the rank 2 intermediate veins that only develop in C_4 leaves are unaffected in mutant leaves (Figures 3, 5, and 6). This phenotypic distinction in mutants is reflected in the spatial distribution of *TML* transcripts during WT development (Figures 2 and S4) and thus regulators that activate *TML* transcription and/or transcript stability determine which procambial cells are subject to TML-mediated suppression. To date, only one TF that binds *in vitro* to the *ZmTML1* promoter has been identified[66] and no function has been assigned to *ZmbHLH105* or any of its orthologs. Although direct activators of TML activity are unknown, at some level the PIN1/auxin traces that precede the formation of all vein ranks[24] must be interpreted differently in procambial initial cells that form the different vein types, leading to TML activity in some but not all of those cells.

Transcriptome comparisons between WT and mutant shoot apices in maize have provided insight into perturbations caused by loss of TML function; however, because *TML* is expressed in just a few cells and only for a short time, the likelihood of identifying direct targets in this dataset is low. Observed perturbations in both auxin and CK pathways (Figures 4 and S4) could be a direct consequence of loss of TML function but there is insufficient spatial resolution in whole-tissue transcriptomes to validate this suggestion. Specifically, the apparent suppression of both pathways observed in whole-shoot apices could be masking significant increases in activity that are spatially or temporally localized. Mechanistically, the presence of an EAR domain[38] in the TML protein is of note because EAR domains bind TOPLESS proteins, which themselves recruit epigenetic modifiers.[37] It is therefore possible that promoters bound by the ZF domain of TML are silenced. Although direct targets have yet to be identified, we propose that TML either represses a target gene that positively regulates lateral vein identity or that TML-mediated regulation of cell divisions in procambial initial cells prevents specific division orientations that are required for lateral vein formation.

Unlike in eudicots, where leaf venation patterning has been perturbed by mutations in genes with specific roles in vein formation (e.g., *cotyledon vascular pattern*[67] and *thickvein*[68]), most known venation defects in grass leaves have resulted from indirect perturbations to hormone pathways, mis-specification of blade versus sheath domains, and/or the regulation of leaf width. For example, growth of maize on auxin transport inhibitors converted blade tissue into sheath, with consequent alterations in vein spacing across the medio-lateral leaf axis.[69] A similar blade to sheath transition was observed in sorghum mutants defective in a cytochrome P450 required for brassinosteroid biosynthesis[70] and in gain-of-function rice mutants that up-regulate CK signaling.[71] In rice, mutants with higher vein density invariably had narrower leaves and smaller mesophyll cells between veins,[72,73] and, in the case of the *narrow leaf 1* mutation, that defect was associated with reduced polar auxin transport.[74] The only mutation reported to directly perturb procambium formation in rice leaves (*radicleless1*), also failed to form an embryonic root.[75] Intriguingly, this pleiotropic phenotype is also observed in the *Arabidopsis* auxin response mutant *monopteros*, despite *MP* being known to play a direct role in leaf vein formation.[55] In contrast with these examples, the role of *TML* in vein development is confined to the leaf, providing an opportunity to manipulate vein patterning in rice for future metabolic engineering of C_4 photosynthesis. An optimal chassis for C_4 engineering would have normal leaf width, vein pairs separated by just two mesophyll cells, and a 1:1 ratio of bundle sheath to mesophyll cells. Loss of TML function does not achieve that goal, however, mutant leaves have a significant increase in the overall volume of leaf veins and in the number of bundle sheath cells. The leaf-specific defects in *Ostml* mutants represent a fundamental advance in our understanding of how veins are patterned in grass leaves and provide a step toward engineering the enhanced vein and bundle sheath cell volume required to underpin C_4 photosynthesis.

STAR★METHODS

Detailed methods are provided in the online version of this paper and include the following:

- KEY RESOURCES TABLE
- RESOURCE AVAILABILITY
  - Lead contact
  - Materials availability
  - Data and code availability
- EXPERIMENTAL MODEL AND SUBJECT DETAILS
  - Plants
  - Microbes
- METHOD DETAILS
  - Phylogenetic analysis

- *In situ* hybridization
- Molecular Cartography probe design
- Tissue preparation and Molecular Cartography hybridization
- Pre-processing of Molecular Cartography images and cell segmentation
- CRISPR target design and cloning
- Overexpression and complementation construct design
- Plant transformation
- DNA extraction
- Genotyping
- Azacytidine (5-azacytidine) treatment
- Phenotyping leaf anatomy
- RNA sequencing, transcript quantification and differential expression
- Differential expression data sub-setting and enrichment analysis
- Enrichment analysis

● QUANTIFICATION AND STATISTICAL ANALYSIS

SUPPLEMENTAL INFORMATION

Supplemental information can be found online at https://doi.org/10.1016/j.cub.2024.03.00.

ACKNOWLEDGMENTS

The authors thank Laurens Pauwels and the VIB team for maize transformation; David Emms for providing the WIP orthogroup sequences; Mara Schuler for making the *ZmUBI*$_{pro}$*:ZmTML* construct; John Baker for plant photography; Roxaana Clayton, Julie Bull, Lizzie Jamison, and Nina Johnson for technical support; and Tom Hughes, Sophie Johnson, Tina Schreier, Sovanna Tan, and Steve Kelly for discussion throughout the experimental work and during manuscript preparation. This research was funded by the Bill and Melinda Gates Foundation C4 Rice grant awarded to the University of Oxford (2015–2019 [OPP1129902] and 2019–2024 [INV-002970]).

AUTHOR CONTRIBUTIONS

D.V., C.P., M.Z., O.S., and J.A.L. conceived and designed the experiments. J.A.L. carried out the phylogenetic analysis (Figures 1 and S1). O.S. performed *in situ* hybridizations (Figures 2 and S2). C.P. and S.B. generated the molecular cartography data (Figures 2, S2, and S4). M.Z. performed the transcriptome analysis (Figures 4 and S4). D.V. carried out all of the remaining experiments. D.V., C.P., M.Z., and J.A.L. analyzed the data. D.V. and J.A.L. wrote the first draft of the manuscript and all authors contributed to the final version.

DECLARATION OF INTERESTS

D.V. and J.A.L. have a pending patent application (PCT/IB2020/056992) related to some of the reported results. S.B. is an employee of Resolve Biosciences, which is the proprietor of Molecular Cartography technology.

Received: December 20, 2023
Revised: February 4, 2024
Accepted: March 7, 2024
Published: March 25, 2024

REFERENCES

1. Meinhardt, H. (2008). Models of biological pattern formation: from elementary steps to the organization of embryonic axes. In Current Topics in Developmental Biology, S. Schnell, P.K. Maini, S.A. Newman, and T.J. Newman, eds. (Academic Press), pp. 1–63. https://doi.org/10.1016/S0070-2153(07)81001-5.
2. Kuhlemeier, C. (2007). Phyllotaxis. Trends Plant Sci. *12*, 143–150. https://doi.org/10.1016/j.tplants.2007.03.004.
3. Perico, C., Tan, S., and Langdale, J.A. (2022). Developmental regulation of leaf venation patterns: monocot versus eudicots and the role of auxin. New Phytol. *234*, 783–803. https://doi.org/10.1111/nph.17955.
4. Roth-Nebelsick, A., Uhl, D., Mosbrugger, V., and Kerp, H. (2001). Evolution and function of leaf venation architecture: a review. Ann. Bot. Lond. *87*, 553–566.
5. Sack, L., and Scoffoni, C. (2013). Leaf venation: structure, function, development, evolution, ecology and applications in the past, present and future. New Phytol. *198*, 983–1000. https://doi.org/10.1111/nph.12253.
6. Jouannet, V., Brackmann, K., and Greb, T. (2015). (Pro)cambium formation and proliferation: two sides of the same coin? Curr. Opin. Plant Biol. *23*, 54–60. https://doi.org/10.1016/j.pbi.2014.10.010.
7. Linh, N.M., and Scarpella, E. (2022). Leaf vein patterning is regulated by the aperture of plasmodesmata intercellular channels. PLoS Biol. *20*, e3001781. https://doi.org/10.1371/journal.pbio.3001781.
8. Sawchuk, M.G., Edgar, A., and Scarpella, E. (2013). Patterning of leaf vein networks by convergent auxin transport pathways. PLoS Genet. *9*, e1003294. https://doi.org/10.1371/journal.pgen.1003294.
9. Govindaraju, P., Verna, C., Zhu, T., and Scarpella, E. (2020). Vein patterning by tissue-specific auxin transport. Development *147*, dev187666. https://doi.org/10.1242/dev.187666.
10. Scarpella, E. (2023). Axes and polarities in leaf vein formation. Plant Physiol. *193*, 112–124. https://doi.org/10.1093/plphys/kiad321.
11. Mattsson, J., Ckurshumova, W., and Berleth, T. (2003). Auxin signaling in Arabidopsis leaf vascular development. Plant Physiol. *131*, 1327–1339. https://doi.org/10.1104/pp.013623.
12. Wenzel, C.L., Schuetz, M., Yu, Q., and Mattsson, J. (2007). Dynamics of MONOPTEROS and PIN-FORMED1 expression during leaf vein pattern formation in *Arabidopsis thaliana*. Plant J. *49*, 387–398. https://doi.org/10.1111/j.1365-313X.2006.02977.x.
13. Donner, T.J., Sherr, I., and Scarpella, E. (2009). Regulation of preprocambial cell state acquisition by auxin signaling in Arabidopsis leaves. Development *136*, 3235–3246. https://doi.org/10.1242/dev.037028.
14. Sawchuk, M.G., Head, P., Donner, T.J., and Scarpella, E. (2007). Time-lapse imaging of Arabidopsis leaf development shows dynamic patterns of procambium formation. New Phytol. *176*, 560–571. https://doi.org/10.1111/j.1469-8137.2007.02193.x.
15. Marcos, D., and Berleth, T. (2014). Dynamic auxin transport patterns preceding vein formation revealed by live-imaging of Arabidopsis leaf primordia. Front. Plant Sci. *5*, 235. https://doi.org/10.3389/fpls.2014.00235.
16. Sharman, B.C. (1942). Developmental anatomy of the shoot of Zea mays L. Ann. Bot. Lond. *6*, 245–282. https://doi.org/10.1093/oxfordjournals.aob.a088407.
17. Russell, S.H., and Evert, R.F. (1985). Leaf vasculature in Zea-Mays-L. Planta *164*, 448–458. https://doi.org/10.1007/BF00395960.
18. Sedelnikova, O.V., Hughes, T.E., and Langdale, J.A. (2018). Understanding the genetic basis of C_4 Kranz anatomy with a view to engineering C_3 crops. Annu. Rev. Genet. *52*, 249–270. https://doi.org/10.1146/annurev-genet-120417-031217.
19. Sage, R.F., Christin, P.-A., and Edwards, E.J. (2011). The C4 plant lineages of planet Earth. J. Exp. Bot. *62*, 3155–3169. https://doi.org/10.1093/jxb/err048.
20. Sharman, B.C., and Hitch, P.A. (1967). Initiation of procambial strands in leaf primordia of bread wheat, Triticum aestivum L. Ann. Bot. Lond. *31*, 229–243. https://doi.org/10.1093/oxfordjournals.aob.a084135.
21. Sakaguchi, J., and Fukuda, H. (2008). Cell differentiation in the longitudinal veins and formation of commissural veins in rice (Oryza sativa) and

maize (Zea mays). J. Plant Res. *121*, 593–602. https://doi.org/10.1007/s10265-008-0189-1.

22. Johnston, R., Leiboff, S., and Scanlon, M.J. (2015). Ontogeny of the sheathing leaf base in maize (Zea mays). New Phytol. *205*, 306–315. https://doi.org/10.1111/nph.13010.
23. Lee, B.H., Johnston, R., Yang, Y., Gallavotti, A., Kojima, M., Travençolo, B.A., Costa, Lda F., Sakakibara, H., and Jackson, D. (2009). Studies of aberrant phyllotaxy1 mutants of maize indicate complex interactions between auxin and cytokinin signaling in the shoot apical meristem. Plant Physiol. *150*, 205–216. https://doi.org/10.1104/pp.109.137034.
24. Robil, J.M., and McSteen, P. (2023). Hormonal control of medial-lateral growth and vein formation in the maize leaf. New Phytol. *238*, 125–141. https://doi.org/10.1111/nph.18625.
25. O'Connor, D.L., Runions, A., Sluis, A., Bragg, J., Vogel, J.P., Prusinkiewicz, P., and Hake, S. (2014). A division in PIN-mediated auxin patterning during organ initiation in grasses. PLoS Comput. Biol. *10*, e1003447. https://doi.org/10.1371/journal.pcbi.1003447.
26. Scarpella, E., Rueb, S., Boot, K.J., Hoge, J.H., and Meijer, A.H. (2000). A role for the rice homeobox gene Oshox1 in provascular cell fate commitment. Development *127*, 3655–3669. https://doi.org/10.1242/dev.127.17.3655.
27. Appelhagen, I., Huep, G., Lu, G.-H., Strompen, G., Weisshaar, B., and Sagasser, M. (2010). Weird fingers: functional analysis of WIP domain proteins. FEBS Lett. *584*, 3116–3122. https://doi.org/10.1016/j.febslet.2010.06.007.
28. Wang, P., Kelly, S., Fouracre, J.P., and Langdale, J.A. (2013). Genome-wide transcript analysis of early maize leaf development reveals gene cohorts associated with the differentiation of C4 Kranz anatomy. Plant J. *75*, 656–670. https://doi.org/10.1111/tpj.12229.
29. Fouracre, J.P., Ando, S., and Langdale, J.A. (2014). Cracking the Kranz enigma with systems biology. J. Exp. Bot. *65*, 3327–3339. https://doi.org/10.1093/jxb/eru015.
30. Emms, D.M., and Kelly, S. (2019). OrthoFinder: phylogenetic orthology inference for comparative genomics. Genome Biol. *20*, 238. https://doi.org/10.1186/s13059-019-1832-y.
31. Sagasser, M., Lu, G.H., Hahlbrock, K., and Weisshaar, B. (2002). A. thaliana TRANSPARENT TESTA 1 is involved in seed coat development and defines the WIP subfamily of plant zinc finger proteins. Genes Dev. *16*, 138–149. https://doi.org/10.1101/gad.212702.
32. Petricka, J.J., Clay, N.K., and Nelson, T.M. (2008). Vein patterning screens and the defectively organized tributaries mutants in *Arabidopsis thaliana*. Plant J. *56*, 251–263. https://doi.org/10.1111/j.1365-313X.2008.03595.x.
33. Du, Y., Roldan, M.V.G., Haraghi, A., Haili, N., Izhaq, F., Verdenaud, M., Boualem, A., and Bendahmane, A. (2022). Spatially expressed WIP genes control Arabidopsis embryonic root development. Nat. Plants *8*, 635–645. https://doi.org/10.1038/s41477-022-01172-4.
34. Vlad, D., and Langdale, J.A. (2022). DEFECTIVELY ORGANIZED TRIBUTARIES 5 is not required for leaf venation patterning in Arabidopsis thaliana. Plant J. *112*, 451–459. https://doi.org/10.1111/tpj.15958.
35. Gaut, B.S. (2001). Patterns of chromosomal duplication in maize and their implications for comparative maps of the grasses. Genome Res. *11*, 55–66. https://doi.org/10.1101/gr.160601.
36. Englbrecht, C.C., Schoof, H., and Böhm, S. (2004). Conservation, diversification and expansion of C2H2 zinc finger proteins in the *Arabidopsis thaliana* genome. BMC Genomics *5*, 39. https://doi.org/10.1186/1471-2164-5-39.
37. Kagale, S., and Rozwadowski, K. (2011). EAR motif-mediated transcriptional repression in plants: an underlying mechanism for epigenetic regulation of gene expression. Epigenetics *6*, 141–146. https://doi.org/10.4161/epi.6.2.13627.
38. Ohta, M., Matsui, K., Hiratsu, K., Shinshi, H., and Ohme-Takagi, M. (2001). Repression domains of class II ERF transcriptional repressors share an essential motif for active repression. Plant Cell *13*, 1959–1968. https://doi.org/10.1105/tpc.010127.
39. Slewinski, T.L., Anderson, A.A., Price, S., Withee, J.R., Gallagher, K., and Turgeon, R. (2014). Short-root1 plays a role in the development of vascular tissue and Kranz anatomy in maize leaves. Mol. Plant *7*, 1388–1392. https://doi.org/10.1093/mp/ssu036.
40. Slewinski, T.L., Anderson, A.A., Zhang, C., and Turgeon, R. (2012). Scarecrow plays a role in establishing Kranz anatomy in maize leaves. Plant Cell Physiol. *53*, 2030–2037. https://doi.org/10.1093/pcp/pcs147.
41. Hughes, T.E., Sedelnikova, O.V., Wu, H., Becraft, P.W., and Langdale, J.A. (2019). Redundant SCARECROW genes pattern distinct cell layers in roots and leaves of maize. Development *146*, e177543. https://doi.org/10.1242/dev.177543.
42. Hughes, T.E., and Langdale, J.A. (2022). SCARECROW is deployed in distinct contexts during rice and maize leaf development. Development *149*, e200410. https://doi.org/10.1242/dev.200410.
43. Hughes, T.E., Sedelnikova, O., Thomas, M., and Langdale, J.A. (2023). Mutations in NAKED-ENDOSPERM IDD genes reveal functional interactions with SCARECROW during leaf patterning in C4 grasses. PLoS Genet. *19*, e1010715. https://doi.org/10.1371/journal.pgen.1010715.
44. Rodriguez, R.E., Mecchia, M.A., Debernardi, J.M., Schommer, C., Weigel, D., and Palatnik, J.F. (2010). Control of cell proliferation in Arabidopsis thaliana by microRNA miR396. Development *137*, 103–112. https://doi.org/10.1242/dev.043067.
45. Nelissen, H., Eeckhout, D., Demuynck, K., Persiau, G., Walton, A., van Bel, M., Vervoort, M., Candaele, J., De Block, J., Aesaert, S., et al. (2015). Dynamic changes in ANGUSTIFOLIA3 complex composition reveal a growth regulatory mechanism in the maize leaf. Plant Cell *27*, 1605–1619. https://doi.org/10.1105/tpc.15.00269.
46. Liu, W.Y., Lin, H.H., Yu, C.P., Chang, C.K., Chen, H.J., Lin, J.J., Lu, M.J., Tu, S.L., Shiu, S.H., Wu, S.H., et al. (2020). Maize ANT1 modulates vascular development, chloroplast development, photosynthesis, and plant growth. Proc. Natl. Acad. Sci. USA *117*, 21747–21756. https://doi.org/10.1073/pnas.2012245117.
47. Nelissen, H., Rymen, B., Jikumaru, Y., Demuynck, K., Van Lijsebettens, M., Kamiya, Y., Inzé, D., and Beemster, G.T. (2012). A local maximum in gibberellin levels regulates maize leaf growth by spatial control of cell division. Curr. Biol. *22*, 1183–1187. https://doi.org/10.1016/j.cub.2012.04.065.
48. De Vos, D., Nelissen, H., AbdElgawad, H., Prinsen, E., Broeckhove, J., Inzé, D., and Beemster, G.T.S. (2020). How grass keeps growing: an integrated analysis of hormonal crosstalk in the maize leaf growth zone. New Phytol. *225*, 2513–2525. https://doi.org/10.1111/nph.16315.
49. Muszynski, M.G., Moss-Taylor, L., Chudalayandi, S., Cahill, J., Del Valle-Echevarria, A.R., Alvarez-Castro, I., Petefish, A., Sakakibara, H., Krivosheev, D.M., Lomin, S.N., et al. (2020). The maize hairy sheath Frayed1 (Hsf1) mutation alters leaf patterning through increased cytokinin signaling. Plant Cell *32*, 1501–1518. https://doi.org/10.1105/tpc.19.00677.
50. Ko, D., Kang, J., Kiba, T., Park, J., Kojima, M., Do, J., Kim, K.Y., Kwon, M., Endler, A., Song, W.-Y., et al. (2014). Arabidopsis ABCG14 is essential for the root-to-shoot translocation of cytokinin. Proc. Natl. Acad. Sci. USA *111*, 7150–7155. https://doi.org/10.1073/pnas.1321519111.
51. Vyroubalová, S., Václavíková, K., Turecková, V., Novák, O., Smehilová, M., Hluska, T., Ohnoutková, L., Frébort, I., and Galuszka, P. (2009). Characterization of new maize genes putatively involved in cytokinin metabolism and their expression during osmotic stress in relation to cytokinin levels. Plant Physiol. *151*, 433–447. https://doi.org/10.1104/pp.109.142489.
52. Lavy, M., and Estelle, M. (2016). Mechanisms of auxin signaling. Development *143*, 3226–3229. https://doi.org/10.1242/dev.131870.
53. Seo, M., Akaba, S., Oritani, T., Delarue, M., Bellini, C., Caboche, M., and Koshiba, T. (1998). Higher activity of an aldehyde oxidase in the auxin-overproducing superroot1 mutant ofArabidopsis thaliana1. Plant Physiol. *116*, 687–693. https://doi.org/10.1104/pp.116.2.687.

54. Przemeck, G.K., Mattsson, J., Hardtke, C.S., Sung, Z.R., and Berleth, T. (1996). Studies on the role of the Arabidopsis gene MONOPTEROS in vascular development and plant cell axialization. Planta *200*, 229–237. https://doi.org/10.1007/BF00208313.

55. Hardtke, C.S., and Berleth, T. (1998). The Arabidopsis gene MONOPTEROS encodes a transcription factor mediating embryo axis formation and vascular development. EMBO J. *17*, 1405–1411. https://doi.org/10.1093/emboj/17.5.1405.

56. Parry, G., Ward, S., Cernac, A., Dharmasiri, S., and Estelle, M. (2006). The Arabidopsis SUPPRESSOR OF AUXIN RESISTANCE proteins are nucleoporins with an important role in hormone signaling and development. Plant Cell *18*, 1590–1603. https://doi.org/10.1105/tpc.106.041566.

57. Galli, M., Khakhar, A., Lu, Z., Chen, Z., Sen, S., Joshi, T., Nemhauser, J.L., Schmitz, R.J., and Gallavotti, A. (2018). The DNA binding landscape of the maize AUXIN RESPONSE FACTOR family. Nat. Commun. *9*, 4526. https://doi.org/10.1038/s41467-018-06977-6.

58. Wang, P., Vlad, D., and Langdale, J.A. (2016). Finding the genes to build C4 rice. Curr. Opin. Plant Biol. *31*, 44–50. https://doi.org/10.1016/j.pbi.2016.03.012.

59. Hibberd, J.M., Sheehy, J.E., and Langdale, J.A. (2008). Using C4 photosynthesis to increase the yield of rice-rationale and feasibility. Curr. Opin. Plant Biol. *11*, 228–231. https://doi.org/10.1016/j.pbi.2007.11.002.

60. Jones, V.A., and Dolan, L. (2017). MpWIP regulates air pore complex development in the liverwort Marchantia polymorpha. Development *144*, 1472–1476. https://doi.org/10.1242/dev.144287.

61. Crawford, B.C.W., Ditta, G., and Yanofsky, M.F. (2007). The NTT gene is required for transmitting-tract development in carpels of *Arabidopsis thaliana*. Curr. Biol. *17*, 1101–1108. https://doi.org/10.1016/j.cub.2007.05.079.

62. Crawford, B.C.W., Sewell, J., Golembeski, G., Roshan, C., Long, J.A., and Yanofsky, M.F. (2015). Plant development. Genetic control of distal stem cell fate within root and embryonic meristems. Science *347*, 655–659. https://doi.org/10.1126/science.aaa0196.

63. Diaz-Ramirez, D., Diaz-Garcia, U.S., Magdaleno-Garcia, G., Huep, G., Appelhagen, I., Sagasser, M., and Marsch-Martinez, N. (2022). Expression and functional analyses of the WIP gene family in Arabidopsis. Plants (Basel) *11*, 2010. https://doi.org/10.3390/plants11152010.

64. Roldan, M.V.G., Izhaq, F., Verdenaud, M., Eleblu, J., Haraghi, A., Sommard, V., Chambrier, P., Latrasse, D., Jégu, T., Benhamed, M., et al. (2020). Integrative genome-wide analysis reveals the role of WIP proteins in inhibition of growth and development. Commun. Biol. *3*, 239. https://doi.org/10.1038/s42003-020-0969-2.

65. Ren, G., Li, L., Huang, Y., Wang, Y., Zhang, W., Zheng, R., Zhong, C., and Wang, X. (2018). GhWIP2, a WIP zinc finger protein, suppresses cell expansion in Gerbera hybrida by mediating crosstalk between gibberellin, abscisic acid, and auxin. New Phytol. *219*, 728–742. https://doi.org/10.1111/nph.15175.

66. Liu, W.-Y., Yu, C.-P., Chang, C.-K., Chen, H.-J., Li, M.-Y., Chen, Y.-H., Shiu, S.-H., Ku, M.S.B., Tu, S.-L., Lu, M.-Y.J., and Li, W.-H. (2022). Regulators of early maize leaf development inferred from transcriptomes of laser capture microdissection (LCM)-isolated embryonic leaf cells. Proc. Natl. Acad. Sci. USA *119*, e2208795119. https://doi.org/10.1073/pnas.2208795119.

67. Carland, F., and Nelson, T. (2009). CVP2- and CVL1-mediated phosphoinositide signaling as a regulator of the ARF GAP SFC/VAN3 in establishment of foliar vein patterns. Plant J. *59*, 895–907. https://doi.org/10.1111/j.1365-313X.2009.03920.x.

68. Clay, N.K., and Nelson, T. (2005). Arabidopsis thickvein mutation affects vein thickness and organ vascularization, and resides in a provascular cell-specific spermine synthase involved in vein definition and in polar auxin transport. Plant Physiol. *138*, 767–777. https://doi.org/10.1104/pp.104.055756.

69. Tsiantis, M., Brown, M.I., Skibinski, G., and Langdale, J.A. (1999). Disruption of auxin transport is associated with aberrant leaf development in maize. Plant Physiol. *121*, 1163–1168. https://doi.org/10.1104/pp.121.4.1163.

70. Rizal, G., Thakur, V., Dionora, J., Karki, S., Wanchana, S., Acebron, K., Larazo, N., Garcia, R., Mabilangan, A., Montecillo, F., et al. (2015). Two forward genetic screens for vein density mutants in sorghum converge on a cytochrome P450 gene in the brassinosteroid pathway. Plant J. *84*, 257–266. https://doi.org/10.1111/tpj.13007.

71. Sakamoto, T., Sakakibara, H., Kojima, M., Yamamoto, Y., Nagasaki, H., Inukai, Y., Sato, Y., and Matsuoka, M. (2006). Ectopic expression of KNOTTED1-like homeobox protein induces expression of cytokinin biosynthesis genes in rice. Plant Physiol. *142*, 54–62. https://doi.org/10.1104/pp.106.085811.

72. Smillie, I.R., Pyke, K.A., and Murchie, E.H. (2012). Variation in vein density and mesophyll cell architecture in a rice deletion mutant population. J. Exp. Bot. *63*, 4563–4570. https://doi.org/10.1093/jxb/ers142.

73. Feldman, A.B., Murchie, E.H.E., Leung, H., Baraoidan, M., Coe, R., Yu, S.M., Lo, S.F., Quick, W.P., Sage, T., and Sage, R. (2014). Increasing leaf vein density by mutagenesis: laying the foundations for C4 rice. PLoS One *9*, e94947. https://doi.org/10.1371/journal.pone.0094947.

74. Qi, J., Qian, Q., Bu, Q., Li, S., Chen, Q., Sun, J., Liang, W., Zhou, Y., Chu, C., Li, X., et al. (2008). Mutation of the rice Narrow leaf1 gene, which encodes a novel protein, affects vein patterning and polar auxin transport. Plant Physiol. *147*, 1947–1959. https://doi.org/10.1104/pp.108.118778.

75. Scarpella, E., Rueb, S., and Meijer, A.H. (2003). The RADICLELESS1 gene is required for vascular pattern formation in rice. Development *130*, 645–658. https://doi.org/10.1242/dev.00243.

76. Kim, C.M., and Dolan, L. (2016). ROOT HAIR DEFECTIVE SIX-LIKE Class I Genes Promote Root Hair Development in the Grass Brachypodium distachyon. PLoS Genet. *12*, e1006211. https://doi.org/10.1371/journal.pgen.1006211.

77. Weber, E., Engler, C., Gruetzner, R., Werner, S., and Marillonnet, S. (2011). A modular cloning system for standardized assembly of multigene constructs. PLoS One *6*, e16765. https://doi.org/10.1371/journal.pone.0016765.

78. Wickham, H. (2009). ggplot2: Elegant Graphics for Data Analysis, Second Edition (Springer), p. 221.

79. Wickham, H., Francois, R., Henry, L., Muller, K.J., and Vaughan, D. (2023). plyr: A Grammar of Data Manipulation. R package version 1.1.4. https://github.com/tidyverse/dplyr.

80. Rueden, C.T., Schindelin, J., Hiner, M.C., DeZonia, B.E., Walter, A.E., Arena, E.T., and Eliceiri, K.W. (2017). ImageJ2: ImageJ for the next generation of scientific image data. BMC Bioinformatics *18*, 529. https://doi.org/10.1186/s12859-017-1934-z.

81. Pachitariu, M., and Stringer, C. (2022). Cellpose 2.0: how to train your own model. Nat. Methods *19*, 1634–1641. https://doi.org/10.1038/s41592-022-01663-4.

82. Tamura, K., Stecher, G., and Kumar, S. (2021). MEGA11: Molecular Evolutionary Genetics Analysis, version 11. Mol. Biol. Evol. *38*, 3022–3027.

83. Collingridge, P.W., and Kelly, S. (2012). MergeAlign: improving multiple sequence alignment performance by dynamic reconstruction of consensus multiple sequence alignments. BMC Bioinformatics *13*, 117. https://doi.org/10.1186/1471-2105-13-117.

84. Trifinopoulos, J., Nguyen, L.T., von Haeseler, A., and Minh, B.Q. (2016). W-IQ-TREE: a fast online phylogenetic tool for maximum likelihood analysis. Nucleic Acids Res. *44*, W232–W235. https://doi.org/10.1093/nar/gkw256.

85. Letunic, I., and Bork, P. (2021). Interactive Tree Of Life (iTOL) v5: an online tool for phylogenetic tree display and annotation. Nucleic Acids Res. *49*, W293–W296. https://doi.org/10.1093/nar/gkab301.

86. Katoh, K., Kuma, K.-i., Toh, H., and Miyata, T. (2005). MAFFT version 5: improvement in accuracy of multiple sequence alignment. Nucleic Acids Res. *33*, 511–518. https://doi.org/10.1093/nar/gki198.

87. Edgar, R., Domrachev, M., and Lash, A.E. (2002). Gene Expression Omnibus: NCBI gene expression and hybridization array data repository. Nucleic Acids Res. *30*, 207–210. https://doi.org/10.1093/nar/30.1.207.

88. Hughes, T.E., and Langdale, J.A. (2020). SCARECROW gene function is required for photosynthetic development in maize. Plant Direct *4*, e00264. https://doi.org/10.1002/pld3.264.

89. Goodstein, D.M., Shu, S., Howson, R., Neupane, R., Hayes, R.D., Fazo, J., Mitros, T., Dirks, W., Hellsten, U., Putnam, N., and Rokhsar, D.S. (2012). Phytozome: a comparative platform for green plant genomics. Nucleic Acids Res. *40*, D1178–D1186. https://doi.org/10.1093/nar/gkr944.

90. Schuler, M.L., Sedelnikova, O.V., Walker, B.J., Westhoff, P., and Langdale, J.A. (2018). SHORTROOT-mediated increase in stomatal density has no impact on photosynthetic Efficiency. Plant Physiol *176*, 757–772. https://doi.org/10.1104/pp.17.01005.

91. Glenn, P., Woods, D.P., Zhang, J., Gabay, G., Odle, N., and Dubcovsky, J. (2023). Wheat bZIPC1 interacts with FT2 and contributes to the regulation of spikelet number per spike. Theor. Appl. Genet. *136*, 237. https://doi.org/10.1007/s00122-023-04484-x.

92. Waisman, A., Norris, A.M., Elías Costa, M., and Kopinke, D. (2021). Automatic and unbiased segmentation and quantification of myofibers in skeletal muscle. Sci. Rep. *11*, 11793. https://doi.org/10.1038/s41598-021-91191-6.

93. Concordet, J.-P., and Haeussler, M. (2018). CRISPOR: intuitive guide selection for CRISPR/Cas9 genome editing experiments and screens. Nucleic Acids Res. *46*, W242–W245. https://doi.org/10.1093/nar/gky354.

94. Ma, X., Zhang, Q., Zhu, Q., Liu, W., Chen, Y., Qiu, R., Wang, B., Yang, Z., Li, H., Lin, Y., et al. (2015). A robust CRISPR/Cas9 system for convenient, high-efficiency multiplex genome editing in monocot and dicot plants. Mol. Plant *8*, 1274–1284. https://doi.org/10.1016/j.molp.2015.04.007.

95. Ricci, W.A., Lu, Z., Ji, L., Marand, A.P., Ethridge, C.L., Murphy, N.G., Noshay, J.M., Galli, M., Mejía-Guerra, M.K., Colomé-Tatché, M., et al. (2019). Widespread long-range cis-regulatory elements in the maize genome. Nat. Plants *5*, 1237–1249. https://doi.org/10.1038/s41477-019-0547-0.

96. Lu, Z., Marand, A.P., Ricci, W.A., Ethridge, C.L., Zhang, X., and Schmitz, R.J. (2019). The prevalence, evolution and chromatin signatures of plant regulatory elements. Nat. Plants *5*, 1250–1259. https://doi.org/10.1038/s41477-019-0548-z.

97. Toki, S., Hara, N., Ono, K., Onodera, H., Tagiri, A., Oka, S., and Tanaka, H. (2006). Early infection of scutellum tissue with Agrobacterium allows high-speed transformation of rice. Plant J. *47*, 969–976. https://doi.org/10.1111/j.1365-313X.2006.02836.x.

98. Finley, T., Chappell, H., and Veena, V. (2021). Agrobacterium-mediated transformation of Setaria viridis, a model system for cereals and bioenergy crops. Curr. Protoc. *1*, e127. https://doi.org/10.1002/cpz1.127.

99. Edwards, K., Johnstone, C., and Thompson, C. (1991). A simple and rapid method for the preparation of plant genomic DNA for PCR analysis. Nucleic Acids Res. *19*, 1349. https://doi.org/10.1093/nar/19.6.1349.

100. Murray, M.G., and Thompson, W.F. (1980). Rapid isolation of high molecular weight plant DNA. Nucleic Acids Res. *8*, 4321–4325. https://doi.org/10.1093/nar/8.19.4321.

101. Kumpatla, S.P., Teng, W., Buchholz, W.G., and Hall, T.C. (1997). Epigenetic transcriptional silencing and 5-azacytidine-mediated reactivation of a complex transgene in rice. Plant Physiol *115*, 361–373. https://doi.org/10.1104/pp.115.2.361.

102. Ewels, P., Magnusson, M., Lundin, S., and Käller, M. (2016). MultiQC: summarize analysis results for multiple tools and samples in a single report. Bioinformatics *32*, 3047–3048. https://doi.org/10.1093/bioinformatics/btw354.

103. Dobin, A., Davis, C.A., Schlesinger, F., Drenkow, J., Zaleski, C., Jha, S., Batut, P., Chaisson, M., and Gingeras, T.R. (2013). STAR: ultrafast universal RNA-seq aligner. Bioinformatics *29*, 15–21. https://doi.org/10.1093/bioinformatics/bts635.

104. Patro, R., Duggal, G., Love, M.I., Irizarry, R.A., and Kingsford, C. (2017). Salmon provides fast and bias-aware quantification of transcript expression. Nat. Methods *14*, 417–419. https://doi.org/10.1038/nmeth.4197.

105. Love, M.I., Huber, W., and Anders, S. (2014). Moderated estimation of fold change and dispersion for RNA-seq data with DESeq2. Genome Biol. *15*, 550. https://doi.org/10.1186/s13059-014-0550-8.

106. Matthes, M.S., Best, N.B., Robil, J.M., Malcomber, S., Gallavotti, A., and McSteen, P. (2019). Auxin EvoDevo: conservation and diversification of genes regulating auxin biosynthesis, transport, and signaling. Mol. Plant *12*, 298–320. https://doi.org/10.1016/j.molp.2018.12.012.

107. Thomas, P.D., Ebert, D., Muruganujan, A., Mushayahama, T., Albou, L.-P., and Mi, H. (2022). PANTHER: making genome-scale phylogenetics accessible to all. Protein Sci. *31*, 8–22. https://doi.org/10.1002/pro.4218.

108. UniProt Consortium (2023). UniProt: the Universal Protein Knowledgebase in 2023. Nucleic Acids Res. *51*, D523–D531. https://doi.org/10.1093/nar/gkac1052.

109. Yilmaz, A., Nishiyama, M.Y., Jr., Fuentes, B.G., Souza, G.M., Janies, D., Gray, J., and Grotewold, E. (2009). GRASSIUS: a platform for comparative regulatory genomics across the grasses. Plant Physiol. *149*, 171–180. https://doi.org/10.1104/pp.108.128579.

STAR★METHODS

KEY RESOURCES TABLE

REAGENT or RESOURCE	SOURCE	IDENTIFIER
Bacterial and virus strains		
Escherichia coli (*E. coli*) DH10B	NEB	Cat#C3019H
Agrobacterium tumefaciens EHA105	Widely distributed	N/A
Agrobacterium tumefaciens AGL1	Widely distributed	N/A
Biological samples		
Zmtml1tml2	This paper	N/A
ZmTML1TML2 (J3)	This paper	N/A
Zmtml1TML2 (J3)	This paper	N/A
Zmwip6A_m1 (J3)	This paper	N/A
Zmwip6A_m2 (B1-10)	This paper	N/A
Zmwip6A_m3 (I20_18)	This paper	N/A
Zmwip6A_m4 (I20_3)	This paper	N/A
Zmwip6B_m1 (J3)	This paper	N/A
Zmwip6B_m2 (I20)	This paper	N/A
Zmwip6B_m3 (I20)	This paper	N/A
Ostml-m1	This paper	N/A
Ostml-m2	This paper	N/A
Ostml-m3.1	This paper	N/A
Ostml-m3.3	This paper	N/A
Ostml-m4	This paper	N/A
Svtml	This paper	N/A
Chemicals, peptides, and recombinant proteins		
½ MS Medium including vitamins	Duchefa Biochem	M0222.0050
Casamino acid	Sigma	C7290
L-proline	Duchefa	P0717.0100
2,4-D	Sigma	D7299
Glucose	Sigma-Aldrich	49152
MES	Sigma-Aldrich	M8250
Potassium hydroxide (KOH)	Sigma-Aldrich	221473
Sorbitol	Melford	S23080
Kinetin	Sigma-Aldrich	48130
ZnSO4	Duchefa	Z0526.0500
CuSO4	Sigma-Aldrich	C3036
Gelzan	Sigma-Aldrich	G1910
5-azacytidine	Sigma-Aldrich	A2385
RNAlater™ Stabilization Solution	Invitrogen	Cat#AM7020
SlowFade Diamond antifade	Invitrogen	Cat#S36972
Acetic anhydride	Sigma-Aldrich	Cat#320102
Ethanol	Merck	Cat# 32221-M
Histoclear	National Diagnostics	Cat# HS-200
Triethanolamine	Sigma-Aldrich	Cat# T5830-0
Paraformaldehyde	Fisher	P/0840/53
Paraplast Plus	Sigma-Aldrich	P3683

(*Continued on next page*)

Continued

REAGENT or RESOURCE	SOURCE	IDENTIFIER
Critical commercial assays		
Gateway BP Clonase II enzyme mix	Invitrogen	Cat#11789020
Gateway LR Clonase II enzyme mix	Invitrogen	Cat#11791100
PCR DIG Probe Synthesis Kit	Roche	Cat#1636090
GoTaq Polymerase	Promega	M7845
RNeasy Plant Mini Kit	Qiagen	Cat#74904
TURBO DNA-free™ Kit	Invitrogen	Cat#AM1907
Qubit™ RNA HS Assay Kit	Invitrogen	Cat#Q32852
Agilent RNA 6000 Nano Kit	Agilent	Cat#5067-1511
TruSeq® Stranded mRNA Library Prep	Illumina	Cat#20020594
Q5 Polymerase	NEB	NEB# M0491L
NEBuilder HiFi DNA Assembly	NEB	NEB# M2621
Deposited data		
Raw and analyzed data	This paper	GEO: GSE255222
Molecular Cartography raw data	This paper and Perico et al. (https://doi.org/10.1101/2024.02.05.578898)	https://doi.org/10.5281/zenodo.10605855
Experimental models: Organisms/strains		
Zea mays L. inbred line B104	VIB Ghent	N/A
Oryza Sativa spp. Japonica cultivar Kitaake	IRRI	N/A
Setaria viridis accession ME034V	Donald Danforth Plant Science Center	ME034V
Sorghum bicolor (L.) Moench subsp. *bicolor* inbred variety 'BTx623'	N/A	N/A
Oligonucleotides		
In situ probe_ZmWIP6A-F:*AATTAACCCTCACTAAAG* GGTAGCTCTCTCTCCCCCATCA (T3 polymerase)	This paper	N/A
In situ probe_ZmWIP6A-R: TAATACGACTCACTATAGGGGGGTGAGCCAAGGG TAAGA (T7 polymerase)	This paper	N/A
In situ probe_ZmWIP6B-F: AATTAACCCTCACTAAAGGGGGAGGAGGACGAC GATGAT (T3 polymerase)	This paper	N/A
In situ probe_ZmWIP6B-R: TAATACGACTCACTATAG GGAAGAGATGCATGAGCAGCAC (T7 polymerase)	This paper	N/A
In situ probe_SvWIP6-F: AATTAACCCTCACTAAAG GGCAGTCCATGCTCCTCCTCTC (T3 polymerase)	This paper	N/A
In situ probe_SvWIP6-R: TAATACGACTCACTATAGG GGCCGTTGTAGTGACTCTGGTG (T7 polymerase)	This paper	N/A
In situ probe_OsWIP6-F: AATTAACCCTCACTAAA GGGCATGCTTCTCCTCTCGCTCT (T3 polymerase)	This paper	N/A
In situ probe_OsWIP6-R: TAATACGACTCACTATA GGGATGGACGCAGACGAGCAC (T7 polymerase)	This paper	N/A
In situ probe_SbWIP6-F: AATTAACCCTCACTAAAG GGTACACTCACCCGTACCAGCA (T3 polymerase)	This paper	N/A
In situ probe_SbWIP6-R TAATACGACTCACTATAGG GGGGGCTATGGACAGTGAGAT (T7 polymerase)	This paper	N/A
Recombinant DNA		
PVec8-Gateway	Kim and Dolan[76]	N/A
Gateway donor vector	Thermo Fisher Scientific	pDONR207
Golden Gate modules including End-linkers, Level 0 and Level 1 vector backbones, EC41421,	Sylvestre Marillonnet Weber et al.[77]	N/A

(*Continued on next page*)

Continued

REAGENT or RESOURCE	SOURCE	IDENTIFIER
pICSL4723	Mark Youles (The Sainsbury Lab, Norwich, UK)	N/A
EC15455 (pZmUbi), EC15216 (pOsACT), EC15069 (HYG)	Ben Miller (University of East Anglia, UK	N/A
EC15768, EC15769	Christian Rogers, ENSA	N/A
Level 0 modules: EC17910, EC17909, EC17912, EC17913	This paper	N/A
Level 1 modules: EC33176, EC33177, EC17736, EC33117, EC33118, EC17738, EC17776, EC17100	This paper	N/A
EC17627, EC17697, EC17847, OsWIP6genomic and OsWIP6genomic_'ATAC'	This paper	N/A
Software and algorithms		
FastQC: a quality control tool for high throughput sequence data.	https://github.com/s-andrews/FastQC.git	http://www.bioinformatics.babraham.ac.uk/projects/fastqc
MultiQC: summarize analysis results for multiple tools and samples in a single report	https://github.com/MultiQC/MultiQC.git	https://doi.org/10.1093/bioinformatics/btw354
STAR: ultrafast universal RNA-seq aligner	https://github.com/alexdobin/STAR.git	https://doi.org/10.1093/bioinformatics/bts635
Salmon provides fast and bias-aware quantification of transcript expression	https://github.com/COMBINE-lab/salmon.git	https://doi.org/10.1038/nmeth.4197
R: A language and environment for statistical	https://cran.r-project.org/bin/macosx/	https://www.r-project.org/
tidyverse; ggplot2	Wickham[78]	https://github.com/tidyverse/ggplot2.git
tidyverse; dplyr	Wickham et al.[79]	https://github.com/tidyverse/dplyr
ImageJ2	Rueden et al.[80]	https://imagej.net/
Cellpose 2.0	Pachitariu and Stringer[81]	https://www.cellpose.org/
OrthoFinder	Emms and Kelly[30]	https://github.com/davidemms/OrthoFinder
MEGA	Tamura et al.[82]	https://mega.io/
MergeAlign	Collingridge and Kelly[83]	http://www.stevekellylab.com/software/mergealign
IQTREE	Trifinopoulos et al.[84]	http://www.iqtree.org/
ITOL	Letunic and Bork[85]	https://itol.embl.de/
MAFFT	Katoh et al.[86]	https://mafft.cbrc.jp/alignment/server/index.html

RESOURCE AVAILABILITY

Lead contact

Further information and requests for resources and reagents should be directed to and will be fulfilled by the lead contact, Jane Langdale (jane.langdale@biology.ox.ac.uk).

Materials availability

Materials generated in this study are available upon request. Please note that the transfer of transgenic lines will be governed by an MTA, will depend on appropriate import permits being acquired by the receiver, and may be constrained by the size of the available seed stocks.

Data and code availability

- The transcriptomes data discussed in this publication have been deposited in NCBI's Gene Expression Omnibus[87] and are accessible through GEO: GSE255222 (https://www.ncbi.nlm.nih.gov/geo/query/acc.cgi?acc=GSE255222).
- The code for the transcriptomes analysis, including all the parameters used, can be accessed on GitHub: https://github.com/mzaidem/TML_Transcriptome_sequencing_processing.git

- Molecular Cartography raw data, cell outlines and DAPI and Calcofluor images are accessible on Zenodo: https://doi.org/10.5281/zenodo.10605855.

EXPERIMENTAL MODEL AND SUBJECT DETAILS

Plants

Oryza Sativa spp. *Japonica* cultivar Kitaake was used to generate gene edited and transgenic lines. All rice plants were grown from seeds germinated in sterile conditions. Dehulled seeds were surface sterilized by gently rocking the seeds in 70 % ethanol (Sigma Aldrich 32221) for 2 min followed by a 15 min treatment with a 25 % sodium hypochlorite solution (Fisher Scientific 5/5040/PB17) supplemented with 0.1 % Tween-20 (Sigma Aldrich P1379). After rinsing the seeds five times with sterile water, they were placed in petri dishes containing half strength MS medium [2.15 g/l Murashige and Skoog salts and vitamins (Duchefa DM0222), 15 g/l sucrose (Sigma Aldrich 16104), 0.5 g/l MES (Sigma Aldrich M8250), 4 g/l Phytagel (Sigma Aldrich P8169), pH 5.8] and germinated in a plant growth cabinet (Panasonic MLR-352-PE) with a 16 h light /8 h dark photoperiod, 30 °C day/ 25 °C night temperatures and approx. 250 μmol photon m^{-2} s^{-1}. Seven days after plating, seedlings were transferred to 50 ml Falcon tubes (Corning 430291) containing 1/4 MS liquid medium [1.1 g/l Murashige and Skoog salts and vitamins, pH 5.8], covered with clingfilm to maintain high humidity until seedlings reached the top of the tube and grown in the same growth cabinet. Two to three-week-old seedlings were transferred to 7.5 cm square pots containing a clay substrate (Profile, Porous Ceramic Topdressing and Construction Material) and grown under the same photoperiod and temperatures described above in a controlled environment chamber (CER) with a light intensity of 250-300 μmol photons m^{-2} s^{-1}. Because the CER is not humidity controlled, to increase the relative humidity around the young plants, the planting trays containing 15 seedlings each were covered with clear plastic bags which were gradually opened at the top after 10 days. Grown in a semi-hydroponic setting plants were watered 3 times per week, once with a fertilizer solution [1.34 g/l Everris Peters Excel Cal-Mag Grower N.P.K. 15-5-15 (pH 5-6)] and twice with room temperature tap water. On alternate weeks the fertilization solution was supplemented with 0.5 g/l chelated iron (pH 6-8, Gardendirect.co.uk) until the plants flowered. A similar protocol was described by Hughes and Langdale.[88]

Zea mays L. inbred line B104 was used to generate the *ZmWIP6* CRISPR lines. Maize plants were grown in a greenhouse with a 16 h light /8 h dark photoperiod with 28 °C day and 20 °C night temperatures. Under low natural light conditions (below 120 μmol photon m^{-2} s^{-1}) plants were provided with supplemental light (Hortilux Schreder, HPS 400 watt). For genotyping, maize seeds were germinated in 24 cell plastic seed trays (Vacapot 24) in a ~ 3 cm layer of damp medium vermiculite (Sinclair Pro) placed on top of a 3:1 mix of John Innes No. 3 Compost (J. Arthur Bower) and medium vermiculite (Sinclair Pro). Seedlings selected for phenotyping and seed set were transferred to 10 L pots containing the same a 3:1 mix mentioned above supplemented with 2.5 g/L Osmocote Exact Standard slow-release fertilizer.

Setaria viridis accession ME034V was used to generate *SvWIP6* edited lines. Plants were grown in the same greenhouse used for maize (see above). To break dormancy prior to germination, the seeds were kept at 4 °C in damp sphagnum moss (Zoo-Med Laboratories Inc) for at least 3 weeks and then dried. To germinate, seeds were placed on top of damp paper towels in sealed petri dishes in a plant growth cabinet (Panasonic MLR-352-PE) with 16 h light /8 h dark photoperiod and 30 °C day/ 25 °C night temperatures. After five days, seedlings were planted into Sinclair compost in 40 cell plastic seed trays (Vacapot 40) and transferred to the greenhouse. Following genotyping selected plants grown for seed propagation or phenotyping were re-potted after 4 weeks into 7.5 cm square pots with the same compost and grown to maturity.

Microbes

Escherichia coli (*E. coli*) DH10B used for cloning were grown on LB medium supplemented with appropriate antibiotic and incubated at 37 °C. Liquid cultures were grown on a shaking incubator set at 180 rpm.

Agrobacterium tumefaciens strains EHA105 and AGL1 used for plant transformation were cultured in LB supplemented with 100 mg/L rifampicin (Duchefa, R0146.0001) plus appropriate antibiotic depending on the construct at 28 °C. Individual colonies were selected on solid LB plates. Liquid cultures were grown on a shaking incubator set at 180 rpm.

METHOD DETAILS

Phylogenetic analysis

For the WIP family tree, the complete set of predicted proteomes for all species in Phytozome version 12[89] were subject to orthogroup inference using OrthoFinder.[30] The orthogroup containing the maize gene GRMZM2G150011(v3 genome)/ Zm00001d020037(v4 genome)/Zm00001eb309530 (v5 genome) was identified and the 379 constituent protein sequences (Data S1) subject to multiple sequence alignment using MergeAlign.[83] The alignment was then imported into MEGA[82] and trimmed to contain the EAR domain plus the zinc finger region. After empirical testing of the multiple sequence alignment for maximum likelihood phylogenetic tree inference using IQTREE,[84] 11 sequences that failed the composition χ^2 test and 21 sequences that had more than 50% gaps were removed. After realignment of the remaining 347 sequences using MergeAlign (Data S2), the best-fitting model parameters (JTT+I+G4) were estimated and a consensus phylogenetic tree was estimated from 1000 bootstrap replicates (Data S2). The data were imported into ITOL[85] to generate the pictorial representation. Branches with less than 50% bootstrap support

were deleted and three leaves that were incorrectly positioned in the WIP2/4/5 clade (likely due to mis-annotation of the corresponding sequences) were deleted (Asparagus v1 05.3078 – positioned in a eudicot clade, *H. annus* chr02g0056311 – positioned in a monocot clade, and *Zostera marina* Zosma112g00240.1 – splitting gymnosperm and Amborella).

For the WIP6 tree, sequences were selected from two bryophytes (to root the tree), 6 eudicots and 7 monocots (Data S1). Species were chosen primarily to resolve relationships within the Panicoid grasses but also to represent the major flowering plant groups (monocots, asterids and rosids). Sequences were retrieved by BLAST searches of Phytozome 13 and NCBI and aligned with MAFFT using the L-INS-i refinement method[86] (Figure S1A; Data S2). IQTree[84] was used to estimate the best-fitting model parameters (JTT+F+I+G4) and to infer a consensus phylogenetic tree from 1000 bootstrap replicates (Data S2). The data were imported into ITOL to generate the pictorial representation. Notably it was extremely difficult to align sequences between the EAR and WIP domains across a broad phylogenetic range, with blocks of sequence conserved within groups (e.g. grasses and brassicas) but highly variant between groups (Figure S1B; Data S2). Despite a high level of sequence conservation across the zinc finger domains, this variability constrained the number and identity of eudicot species for which tree inference was supported with high bootstrap values.

In situ hybridization

In situ hybridization was carried out using wax-embedded shoot apices as previously described[90]. Maize, rice, sorghum and setaria shoot apices were harvested on ice and immediately placed in freshly prepared fixative solution (4 % (w/v) paraformaldehyde solution with 0.1 % tween-20 and 0.1 % triton-x-100). Samples were vacuum infiltrated (~500 mm Hg) on ice in the fume hood until samples sunk, transferred to fresh solution and fixed overnight at 4 °C. Following fixation, samples were dehydrated using an ice-cold graded ethanol series (10 %, 30 %, 50 % and 70 %) before transferring to a Tissue Tek VIP processor (Sakura, www.sakura.eu) for tissue clearing and wax infiltration. Samples were then embedded in Paraplast Plus (Sigma-Aldrich) and sectioned. Transverse 8 μm sections were mounted on pre-coated slides BDH (Cat. No. 406/0178/00), dried overnight and then treated with Histoclear (National diagnostics) twice for 10 min followed by a 1 min 100 % ethanol wash to remove the embedding medium. Sections were passed through an ethanol series (100 %, 95 %, 85 %, 50 % and 30 %) for 30 s at each concentration followed by 2 min in 0.85 % (w/v) sodium chloride. After a 2 min rinse in 1 x phosphate buffered saline (PBS), samples were incubated with Proteinase K (125 μg/ml) in pre-warmed protease buffer (100 mM Tris pH 8.0, 50 mM EDTA) for 30 minutes at 37 °C and then treated with 0.2 % glycine in 1 x PBS for 2 min to inactivate the proteinase. Samples were rinsed in 1 x PBS for 2 min, re-fixed in 4 % paraformaldehyde solution for 10 min and rinsed twice more in 1 x PBS (2 min each time) before treating with acetic anhydride in 0.1 M triethanolamine pH 8.0. The required volume (depending on the number of slides to be treated) of 0.1 M triethanolamine solution pH 8.0 was prepared by diluting 2 M triethanolamine stock (29.8g in 100ml milli-Q H_2O, pH 8.0 with HCl) in a glass container placed on a magnetic stirrer. After ensuring that the solution could be stirred after the addition of the slide rack to the container, 5 μl acetic anhydride/ml 0.1 M triethanolamine solution pH 8.0 was added and the slides were incubated for 10 min stirring slowly. The slides were rinsed for a final time in PBS for 2 min, dehydrated through the reverse ethanol series (30 %, 50 %, 85 %, 95 % and 100 %), washed in fresh 100 % ethanol and left to dry at room temperature wrapped in paper towels.

Hybridization was carried out with digoxygenin (DIG)-labelled RNA probes designed to specifically detect *ZmWIP6A, ZmWIP6B, OsWIP6, SbWIP6* or *SvWIP6* transcripts. The *ZmWIP6A* probe was a 427 bp fragment spanning 141 bp of the 5'UTR and the first 286 bp of the coding sequence. The probe shared 53 % similarity with the corresponding region of the *ZmWIP6B* transcript sequence. The *ZmWIP6B* probe was a 203 bp fragment encompassing the end of the coding sequence and part of the 3′UTR. The probe shared 52 % similarity with the corresponding region of the *ZmWIP6A* transcript sequence. The *OsWIP6* (142 bp), *SbWIP6* (393 bp) and *SvWIP6* (214 bp) probes encompassed the beginning of the first exon and included the EAR domain.

The probe sequences were PCR amplified using primers appended with T3 and T7 RNA polymerase-binding sites and then labelled using the following reaction mix: 1× RNA polymerase buffer, 0.5 mM ATP, 0.5 mM GTP, 0.5 mM CTP, 0.1 mM digoxigenin-UTP, 0.8 units μL^{-1} RNA polymerase (all Thermo Scientific), and 1.6 units μL^{-1} RNAseOUT (Invitrogen). The reaction was incubated for 1.5 h at 37 °C and terminated by 10 min of incubation at 37 °C with 3 volumes of DNase solution (10 mM Tris-HCl, pH 7.5, 10 mM magnesium chloride, 50 mM sodium chloride, 2.5 μg μL^{-1} tRNA, and 0.02 units μL^{-1} DNase I).

To prepare 800 μl hybridization buffer (sufficient for approx. 20 slides; needs to be empirically determined) the following solutions were mixed: 100 μl 10 x *in situ* hybridization salts (3 M NaCl, 100 mM Tris-HCl pH 8.0, 100 mM Na Phosphate pH6.8, 50 mM EDTA), 400 μl deionized formamide, 10 μl 100mg/ml tRNA, 20 μl 50 x Denhardt's, 200 μl 50 % dextran sulphate, and 70 μl H_2O. Note: preheating dextran sulphate to 60 °C makes pipetting easier. Probes were thawed on ice, mixed with equal volumes deionized formamide (10 μl probe plus 10 μl deionized formamide per slide, empirically determined as too much probe will increase the background signal), incubated at 80 °C for 2 min centrifuged briefly and immediately cooled on ice. Probe was then mixed with the hybridization buffer in a 4:1 buffer: probe ratio. The probe/hybridization buffer mix was added to the slides, after making sure slides are completely dry, and gently covered with a coverslip avoiding bubbles and checking that sections are covered with the hybridization mix. Slides were laid flat in a preheated (above 55 °C) humidity chamber/ hybridization box fitted with supports for the slides, the box was sealed and incubated at 55 °C overnight. Post-hybridization washes were undertaken with 0.05 x SSC buffer made from a 20 x SSC stock (3 M NaCl, 0.3 M Na_3citrate), calculated to ensure stringency. Slides were dipped one at a time into wash buffer pre-warmed at 55 °C (best prepared the previous day and kept at 55 °C) and gently agitated to remove coverslips then gently transferred to a rack and washed twice with 0.05 x SSC, incubating at 55 °C without shaking, for 30 min in the first wash and a further 1 h and a half in the second wash. Slides were then washed twice for 5 min at 37 °C with buffer NTE (0.5 M NaCl, 10 mM Tris-HCl pH7.5, 1 mM EDTA pH8.0, prepared in advance from a 10 x stock solution and pre-warmed at 37 °C) and incubated for 30 min at 37 °C in buffer NTE

containing 20 μg/ml RNaseA (Sigma-Aldrich, R4875). The RNase solution was rinsed off in three 5 min washes with buffer NTE at 37 °C, incubated for 1 h in 0.05 x SSC buffer at 55 °C and further washed for 5 min in PBS at room temperature to prepare for blocking and antibody staining. Signal detection was performed using anti-digoxigenin-AP FAB fragments (Roche #1093-274), 1 in 3000 freshly prepared dilution followed by staining with NBT (4-nitro-blue-tetrazolium chloride)/BCIP (5-bromo-4-chloro-idolyllphosphate 4 toluidine salt) (Roche, 1169-7471001). When signal became apparent (after 12 to 36 h) slides were washed for 1 min with the following solutions: milli Q water, 70 % ethanol, 95 % ethanol, 100 % ethanol, 95 % ethanol, 70 % ethanol and milli Q water. Following counterstaining for 5 min with 0.1 % (w/v) Calcofluor White (Sigma-Aldrich, Fluorescent Brightener 28), slides were mounted in Entellan (Merck Millipore) and imaged under bright-field and UV light using a Leica DMR8 microscope and a QImaging MicroPublisher (QImaging) camera.

Molecular Cartography probe design

Probes were designed using Resolve BioSciences' proprietary design algorithm and gene annotations from the Zea Mays RefGen V4. The final set of probes was selected with the methodology described in Glenn et al.[91]

Tissue preparation and Molecular Cartography hybridization

Wild-type B73 seeds were germinated and grown in an environment-controlled chamber on a 16 h/8 h day/night cycle, temperature 28 °C/20 °C, 50 % humidity and light intensity of 300 μmol m^{-2} s^{-1}. Seeds were germinated in medium vermiculite and seedlings were harvested ten days after sowing. Maize shoot apices were cut just below and 0.5 cm above the shoot apical meristem and immediately transferred to ice-cold 4 % paraformaldehyde supplemented with 0.03 % Triton X-100. Vacuum was applied for 10 min or until complete sinking of the samples to allow for fixation. Samples thus prepared were then dehydrated and embedded in Paraplast Plus following the user guide for sample preparation from Resolve BioSciences. Clearing and wax infiltration were either carried out manually (samples E1B2, E1D2, S1B1 or S1B2) or in a TissueTek VIP processor (samples S1A1, S1A2). Wax-infiltrated samples were embedded in blocks of Paraplast Plus using a TissueTek TEC wax-embedding centre. A total of six 10 μm transverse sections across two experiments were cut with a microtome and baked onto a Molecular Cartography-compatible slide at 37 °C overnight to allow for sample attachment. Sections were then deparaffinized, permeabilized, and refixed according to the user guide. After complete dehydration, the sections were mounted using SlowFade -Diamond Antifade mounting medium, covered with a glass coverslip and shipped to Resolve BioSciences for analysis.

At Resolve BioSciences, sections were washed twice in phosphate buffered saline for 2 min, followed by 1 min washes in 50 % and 70 % ethanol at room temperature. Ethanol was removed by aspiration and DST1 buffer was added, followed by tissue priming for 30 min at 37 °C and by a 48 h hybridization using probes specific for the target genes. Samples were washed to remove excess probes and fluorescently tagged in a two-step color development process. Fluorescent signals were removed after imaging in a decolorization step. Colorization, imaging, and decolorization were iterated for multiple cycles to generate a unique combinatorial code for each target gene. Samples were imaged by Resolve BioSciences as described in Glenn et al.[91] Two independent experiments were carried out: the first with sections E1B2 and E1D2, the second with sections S1A1, S1A2, S1B1, S1B2.

Pre-processing of Molecular Cartography images and cell segmentation

Cell segmentation was carried out using CellPose 2.0,[81] starting from high resolution images of Calcofluor and DAPI-stained sections. A pre-processing step was carried out to facilitate cell segmentation. Firstly, DAPI and Calcofluor images were overlaid in ImageJ2[80]: The overlay of cell wall and nuclear staining allows for more accurate segmentation with CellPose 2.0. Subsequently, different stages of leaf development were cropped and isolated from the overlay image: this allows for faster computational speed during the segmentation step, and for a more accurate estimate of the average cell diameter, which varies greatly between leaf primordia. Images of isolated leaf primordia were imported into CellPose 2.0, and the Calcofluor and DAPI channels brightness and contrast were adjusted as required. The ''cyto2'' model was used to predict the cell boundaries in meristem, P1 and P2 primordia, whereas the "TN2" model was used to predict cell boundaries in P3, P4 and P5 primordia. All segmentations were then manually corrected, and the resulting masks were used to train a custom model. All subsequent primordia underwent segmentation using the custom models thus obtained and corrected manually where required. Segmented cells were exported as PNG masks, converted to ROIs in ImageJ2 with the ''Labels to ROIs'' plugin[92] and ROIs from individual primordia were joined to obtain final images. ROIs were then used to visualize single-cell gene expression using the proprietary Polylux plugin from Resolve Biosciences.

CRISPR target design and cloning

To generate the CRISPR constructs, short RNA guides targeting *ZmWIP6A, ZmWIP6B, SvWIP6 and OsWIP6* were designed using the online guide RNA selection tool, CRISPOR.[93] For maize and setaria, two guide RNAs were designed to target each *WIP6* gene within the first exon. In the case of *OsWIP6* three guides were used, sgRNA1 and sgRNA3 in the first exon and sgRNA4 in the 3'UTR, to potentially generate large deletions in combination with the first two guides.

The four maize guides targeting *ZmWIP6A* (sgRNA25: TGGTACGAGTGATGAGTGTA & sgRNA194: CGCAGCCGGCATTAT TGTAA) and *ZmWIP6B* (sgRNA28: TGCTGGTACGGGTGAGCGTA & sgRNA309: CAGATCCGCCGCCATTGTAA) were cloned in proprietary level 2 vector pMHb-pZmUBIL-ZmCas9-NosT-AG-pBdEF1a-tdTomato-NLS-NosT (https://gatewayvectors.vib.be/).

The rice and setaria sgRNAs were cloned downstream of the OsU3 promoter in the Golden Gate system[77] as previously described.[42] Complementary oligonucleotides containing the sgRNA, flanking 4 bp Golden Gate compatible overhangs and Esp3I restriction sites were obtained by synthesis. Prior to cloning, oligonucleotide pairs were mixed in a 1:1 ratio (8 ml Milli-Q water plus 1 ml each 100mM oligo solution), heated to 99 °C for 5 min and then allowed to cool for 1 h at room temperature for oligonucleotide duplexes to form. The resulting duplexes were diluted 200-fold and used for cloning into level 1 guide RNA scaffold-containing vectors under the control of the OsU3 promoter. The level 1 vectors used were either in position 3 reverse (EC15768), position 4 reverse (EC15769) or position 5 reverse (EC17776) to accommodate the hygromycin resistance cassette, OsACT::HYG in position 1 reverse (EC17100) and the Cas9p cassette in position 2 reverse (EC17738). The *Cas9p* gene[94] was expressed from the *ZmUbi* promoter (EC15455). Both the hygromycin resistance cassette and Cas9 cassette used the t-NOS terminator (EC41421). Level 1 modules were assembled into the level 2 backbone vector pICSL4723 using appropriate Golden Gate end-linkers to generate the final constructs used for plant transformation.

Following the procedure described above the two setaria guides sgRNA77: CTCATCCTACTCGGCATGCT (EC33176, position 3, reverse) and sgRNA153: CCGTTCCCCCCAGCAACAAG (EC33177, position 4, reverse) were assembled into level 2 construct EC17847. The rice guides were used to generate two separate level 2 constructs, EC17627 containing only sgRNA1: TTCAACCCG AGCCACTACCA (EC17736, position 3, reverse) and construct EC17697 containing sgRNA1, sgRNA3: CACCTGTACCAGAG CCACCA (EC33117, position 4, reverse) and sgRNA4: CGTACAGTCTAGCTAGGTAT (EC33118, position 5, reverse).

Overexpression and complementation construct design

The *pZmUbi*: *ZmTML1* overexpression construct was obtained by cloning the *ZmTML1* ORF into the binary destination vector pVec8-Gateway.[76] *The ZmTML1* ORF was amplified by polymerase chain reaction (PCR) using maize B73 genomic DNA as template and Gateway® compatible primers (MS. F: 5'-TCAGCAGACCACCACCCAAT-3'; MS. R: 5'-CTAGATGACGACCATGTCGCTGG-3'). The PCR product was cloned into Gateway® donor vector pDONR™207, sequenced, and subsequently cloned downstream of the *ZmUBI* promoter in the binary destination vector pVec8-Gateway.

The *pZmTML1: ZmTML1* construct was cloned using the Golden Gate system which required any BpiI or BsaI enzyme recognition sites to be domesticated. Both the promoter sequence (EC17047, level 0 'PU' module) (Data S4) and the ZmTML1 CDS (EC17008, Level 0 'SC' module) were domesticated and obtained by synthesis. The assembled level 1 module used the t-NOS terminator (EC41421) assembled into GG level 2 vector (pICSL4723). The hygromycin selection module (EC17117) was used for 'in planta' selection.

OsTML complementation constructs 1, 2 and 3 were also cloned into the Golden Gate system. The *OsTML* CDS (EC17910, level 0 'SC' module) was obtained by synthesis and had one BpiI site 'domesticated'. The 2945 bp promoter region (EC17909, level 0 'PU' module), *OsTML* terminator region (EC17912, level 0 'T' module) and the 3' UTR plus t-NOS (EC17913, level 0 'T' module) were cloned from PCR amplified fragments. As the *OsTML* promoter contained two BsaI and one BpiI enzyme recognition site, primers were designed to introduce 3 single bp changes to 'domesticate' the restriction sites and to add BpiI sites to allow promoter assembly, without introducing any other scars in the sequence. The *OsTML* terminator region and 3'UTR did not require domestication. The resulting level 0 modules were assembled as 'PU'+ 'SC' + 'T' into level 1 modules to obtain complementation constructs 1-3 described in Figure 5D and cloned into GG level 2 vector (pICSL4723) with the hygromycin selection module (EC17117) and appropriate end-linkers.

To avoid any modification that could potentially alter promoter function, the fourth version of the complementation construct was assembled using NEBuilder HiFi DNA Assembly strategy (NEB #E2621). A ~7 kb genomic region, containing ~5 kb regulatory region, the ORF and 3'UTR, was amplified using PCR (polymerase chain reaction) in four overlapping fragments. The four PCR fragments plus a t-NOS terminator were assembled into a GG level 2 vector containing a hygromycin selection module (EC17117) expressed from the maize ubiquitin promoter. To obtain complementation construct 5 (the 'ATAC' version) construct 4 was cut with PmeI and FspI to remove most of the promoter sequence apart from the 545 bp adjacent to the ATG, and a PCR amplified 540 bp fragment overlapping the predicted 'ATAC' region was added via a NEBuilder HiFi DNA Assembly reaction. The ATAC sequence information for both maize[95] and rice[96] was accessed via the Plant Epigenome Browser -https://epigenome.genetics.uga.edu/PlantEpigenome/index.html. Primer sequences for Golden Gate and NEBuilder HiFi DNA Assembly are listed in Table S1. All PCR fragments were amplified using the Q5® High-Fidelity DNA Polymerase (NEB #M0491S).

Plant transformation

Maize CRISPR lines were generated in inbred line B104 at the VIB Ghent Crop Genome Engineering Facility (https://www.psb.ugent.be/cores/crop_genome_engineering_facility). Backcrossed T1 seeds were provided for 10 independent lines.

Transgenic rice (*O. sativa ssp. japonica* cv. Kitaake) lines were obtained following a modified callus transformation protocol from Toki et al.[97] The modified protocol is available at https://langdalelab.files.wordpress.com/2015/07/kitaake_transformation_2015.pdf. To obtain embryogenic callus, mature rice seeds were dehulled and sterilized as described above in the 'Plants' section. After the last wash, sterilized seeds were inoculated on plates containing 45 – 50 ml R1 medium (4.4 g/L Murashige and Skoog salts and vitamins, 30 g/L Sucrose, 0.5 g/L MES, 300 mg/L Casamino acid, 2.8 g/L L-Proline, 2 mg/L 2′4-D, 4 g/L Phytagel, pH 5.8 with 0.1M KOH) and cultured under continuous light at 32 °C for 3 weeks. Formed calli were transferred to fresh R1 plates and cultured for one more week before Agrobacterium transformation.

A single colony of Agrobacterium (strain EHA105) harbouring the binary vector intended for transformation was inoculated in 10 ml LB supplemented with 100 mg/L rifampicin and 50 mg/L kanamycin (for all Golden Gate derived constructs) or 50 mg/L Spectinomycin (for the overexpression construct in pVec8-Gateway binary vector) and grown overnight at 28 °C. Cultures were pelleted by spinning at 4000 rpm for 15 min and pellets were resuspended in sterile AAM medium (4.4 g/L Murashige and Skoog salts and vitamins + 68.5 g/L sucrose + 0.5 g/L MES + 36 g/L glucose + 500 mg/L casamino acid + 100 ml 10 x AA amino acids stock solution, pH 5.2 with KOH) supplemented with 2ul/ml 20mg/ml acetosyringone (Sigma-Aldrich, D134406) to yield an OD600 of approximately 0.5 and kept for 1 h in the flow hood. The 10 x AA amino acids stock solution was prepared by dissolving 8.76 g L-Glutamine, 2.66 g L-Aspartic acid, 1.74 g L-Arginine and 75 mg Glycine.

For transformation calli were immersed in the agrobacterium suspension for 5 min with gentle shaking, then blot dried on sterilized filter paper placed in petri dishes to remove excess bacteria. The infected calli were then transferred R2 medium (4.4 g/L Murashige and Skoog salts and vitamins, 30 g/L Sucrose, 0.5 g/L MES, 300 mg/L Casamino acid, 10 g/L Glucose, 2 mg/L 2′4-D, 4 g/L Phytagel, pH 5.2 with 0.1M KOH and 20 mg/l acetosyringone added after autoclaving) plates, on top of sterilized filtered paper, and cultured in the dark at 25 °C for 3 d. Following co-cultivation calli were transferred to plates containing selective R3 medium [R1 medium supplemented with 200 mg/L Timentin (Melford, T36000) and 30 mg/L Hygromycin B (Melford, H75020) after autoclaving] and cultured under continuous light at 32 °C for 2 weeks. Surviving calli were subcultured to new selective plates and grown for another 2 weeks before moving to regeneration medium, R4 (4.4 g/L Murashige and Skoog salts and vitamins, 30 g/L Sucrose, 0.5 g/L MES, 2 g/L casamino acid, 30 g/L Sorbitol, 2 mg/L kinetin, 1 mg/L NAA, 4 g/L Phytagel, pH 5.8 with 0.1M KOH) supplemented with 200 mg/L Timentin and 20 mg/L Hygromycin B after autoclaving. Culture on regeneration plates until plantlets emerge from calli, transferring regenerating calli to new R4 plates after every 2 weeks of cultivation. When seedlings had roots and were large enough to handle, they were transferred to 50 ml Falcon tubes containing 1/4 MS liquid medium and grown as described in the '*Plants*' section until ready to genotype.

Setaria viridis ME034V plants were transformed using a modified transformation protocol[98] as previously described by Hughes et al.[43] ME034V seeds (>6 months old so no longer dormant) were dehulled and sterilised in a 10 % sodium hypochlorite solution with 0.1 % Tween-20 for 3 min, gently rocking the tube. Seeds were rinsed three times with sterile water before being placed on plates containing callus induction media (CIM) (4.4 g/L Murashige and Skoog salts and vitamins, 40 g maltose, 35 mg/L $ZnSO_4{\cdot}7H2O$, 0.6 mg/L $CuSO_4{\cdot}5H_20$, 0.5 mg/L kinetin, 2 mg/L 2,4-D 4 g/L Gelzan, pH 5.8). A total of 16 seeds with the embryo facing up were placed on each plate and cultured in the dark at 24 °C for 4–5 weeks until embryonic callus was formed. Seedling structures and any gelatinous callus were then carefully removed using a dissecting microscope to select the best quality embryonic callus to subculture onto fresh CIM. After 3 weeks any gelatinous callus formed was again carefully removed under a dissecting microscope and up to 20 2-3 mm callus pieces per plate were moved to fresh medium for 1–2 weeks prior to transformation. For transformation, Agrobacterium strain AGL1 containing the construct of interest was grown overnight, at 28 °C and 125 rpm, in LB liquid media containing with 100 mg/L rifampicin and 50 mg/L kanamycin to an approximate OD_{600} of 0.6. Agrobacteria were then collected by centrifugation at 8000 rpm for 10 min and resuspended by vortexing in 50 ml liquid CIM media supplemented with 40 μM acetosynringone and 0.02 % Pluronic F-68 (product # 092750049, MP Biomedicals). Around 100 pieces of callus were immersed in the Agrobacterium suspension and incubated for 5 min with gentle rocking. The liquid was removed with a pipettor and calli were transferred to fresh CIM plates with sterile filter paper placed on top of the media. Following co-cultivation for 3 days at 22 °C in the dark, calli were transferred to CIM selective plates (CIM containing 150 mg/L timentin (Plant Media) and 40mg/L hygromycin B (H385, PhytoTechnology Laboratories), added after autoclaving from sterile stocks) and kept for 16 d at 24 °C in the dark. Calli were then transferred to plant regeneration media (PRM) (4.4 g/L Murashige and Skoog salts and vitamins, 20 g/L sucrose, 7 g/L Phytoblend (PTP01, Caisson Labs), 2 mg/L kinetin, 150 mg/L timentin, 15 mg/L hygromycin, pH 5.8), grown in plant growth cabinet (Panasonic MLR-352-PE) at 24°C under light conditions (16 h light /8 h dark photoperiod) and moved to fresh media every 2 weeks until shoots appeared. Regenerated 2-3 cm shoots were detached from calli and moved to plates containing rooting media (RM) (2.2 g/L Murashige and Skoog salts and vitamins, 30 g/L sucrose, 7 g/L Phytoblend, 150 mg/L timentin, 20 mg/L hygromycin B, pH 5.7). Shoots that developed healthy roots at this stage were transferred to compost (see 'Plants') for genotyping.

DNA extraction

Genomic DNA was purified from rice, maize or setaria leaves using an SDS based DNA extraction buffer [Edwards Solution: 200 mM Tris-HCl (pH 7.5), 250 mM NaCl, 25 mM EDTA, and 0.5% SDS[99]]. Leaf segments (1-2cm) were harvested from young plants and placed in 1,5 ml Eppendorf tubes with 200 μl DNA extraction buffer and one stainless steel 4mm bead (steamfittings.co.uk). Samples were processed in a tissue lyser (Qiagen Tissuelyser II) at maximum rpm for 1- 2 minutes or until samples were disrupted and the solution turned green. Tubes were then centrifuged for 10 min at max speed in a bench top centrifuge, the supernatant was recovered and transferred to clean Eppendorf tubes containing an equal volume of isopropanol. After mixing, the samples were kept at room temperature for 10 min for the DNA to precipitate and then centrifuged for 10 min at maximum speed. The supernatant was discarded, the pellets were washed with 70 % ethanol and dried at room temperature before resuspending in 100 μl milli Q water.

For genes that were challenging to amplify by PCR, leaf genomic DNA was extracted using a modified cetyl-trimethyl-ammonium bromide (CTAB) protocol optimized to yield high-quality DNA.[100] Tissue was homogenized at room temperature in CTAB buffer [1.5 % (w/v) CTAB, 75 mM Tris-HCl (pH 8), 15 mM EDTA pH 8, 1.05 M NaCl] and incubated at 65 °C for 30 min. Equal volumes of 24:1 chloroform: isoamyl alcohol was added to the samples, mixed, and centrifuged for 15 min at maximum speed in a bench top centrifuge. The resultant supernatant was carefully transferred to fresh tubes and mixed with equal volumes of isopropanol to precipitate

the DNA. DNA was collected by 15 min centrifugation, the pellet was washed with 70 % (v/v) ethanol, dried and resuspended in 100 μl milli Q water. A similar protocol was described by Hughes et al.[41] The same CTAB based DNA extraction was used to extract DNA from maize seed chips for genotyping.

Genotyping

Rice and setaria T0 plantlets regenerated from tissue culture were verified by PCR with primers targeting the selection gene hygromycin phosphotransferase (hpt) (forward primer: 5'- CAACCAAGCTCTGATAGAGT- 3'; reverse primer: 5'- GAAGAATCTCGTGCT TTCA-3') to confirm successful transgene insertion in the genome. The same PCR was used to validate positive transgenic lines in later generations (T1, T2) and select gene edited (CRISPR) T1 progeny free of transgene.

To detect CRISPR induced mutations in T0 lines and to select homozygous plants in subsequent generations, primers were designed to specifically to amplify the WIP6 gene fragment targeted by the short RNA guides. Maize genes *WIP6A* and *WIP6B* were genotyped with primer pairs ZmWIP6A_CRISPR-F: 5'-GAATTTCTGGCCGGTCGATC-3' /ZmWIP6A_CRISPR-R: 5'-CGGTTGAA GGTCTTGTTGCA-3' and ZmWIP6B_CRISPR-F: 5'-TCACTGAATTTTCTGGTCGCC-3' /ZmWIP6B_CRISPR-R: 5'-CTACCAGGATCT CGGAGGC-3' and the SvWIP6 with primers SvWIP6_sg56-F: 5'-CACTTGTTTCTCCCCTCCCT-3' and SvWIP6_sg153-R: 5'TGTAGTG ACTCTGGTGGTGG-3'. For *OsWIP6*, because the guides were spanning a much larger fragment, primers OsWIP6-F: 5'-GGCAGTGAGATCGAGATGGA-3' and OsWIP6-R: 5'-CTGCCTAGCCT AGCCATCTA-3' were used to amplify the whole fragment and internal primers OsWIP6-F3: 5'-AGTCCATGCTTCTCCTCTCG-3' andOsWIP6-R3: 5'-CGGTTGAAGGTCTTGTTGCA-3' were used for sequencing. The resultant amplicons were either digested with a restriction enzyme predicted to cut at the intact guide site or sent for sanger sequencing when no restriction site was available. All PCR amplification reactions used for genotyping used GoTaq DNA polymerase (Promega).

Azacytidine (5-azacytidine) treatment

For treatment with azacytidine, rice seeds were sterilized and germinated on half strength MS medium (described above) containing 50 mg/l 5-azacytidine (A2385, Sigma, dissolved in dimethyl sulfoxide) and in control conditions (1/2 MS containing the equivalent amount of in dimethyl sulfoxide). When seedlings were large enough to handle, they were transferred to pots containing clay and grown as described above until ready for phenotyping. Azacytidine treated seedlings developed much more slowly than controls and not all survived. Azacytidine acts by inhibiting DNA methylase activity and affecting methylation of the whole genome, including transgenes[101].

Phenotyping leaf anatomy

Leaf segments (3-4 mm) spanning the whole leaf width were collected from the widest part of fully expanded leaves, which in maize and setaria localized to the middle of the blade and in rice to the upper third of the blade. Leaf seven was analysed in rice, and leaf five in maize and setaria.

To image young leaf primordia, emerging seedlings of maize (~ 2.5 cm) and rice (3-4 cm) were harvested. The shoot apical meristem and early leaf primordia will be located at the very base of the seedling. Rice root fragments of ~1 cm were sampled from the tips of primary roots of young seedlings. Rachis fragments (~1 cm) just below the first inflorescence branch and pedicels connecting the spikelets to inflorescence branches were sampled just before anthesis.

All samples mentioned above were fixed in 3:1 ethanol: acetic acid for 30 min at room temperature and moved to 70 % ethanol before transferring into tissue embedding cassettes (M491-9, Simport), for processing in a Tissue Tek VIP processor (Sakura, www.sakura.eu). For leaf paradermal sections, fragments of rice leaf blades without the midvein were flattened on a glass microscope slide and stacked using 0.8 % agarose layers to prevent bending during wax embedding. Root samples were also set in 0.8 % agarose before placing in the Tissue Tek processor for similar reasons. Wax infiltrated samples were then embedded in Paraplast Plus and sectioned using a Leica RM2135 rotary microtome. Transverse sections 10 μm thick were obtained for leaf, root, rachis and pedicel samples, whilst 8 μm thick paradermal leaf sections and young primordia transverse sections were necessary. Sections were placed onto microscope slides and dried at 37 °C overnight before dewaxing and staining.

Leaf sections were treated with Histoclear twice for 5 min followed by two 100 % ethanol 1 min washes to remove the wax. Sections were then partially rehydrated in 70 % EtOH for 1 min prior to staining for 30 min with Safranin O (1 % in 50 % EtOH), rinsed in 70 % ethanol and stained for 30 s with Fast Green FCF (0.03 % in 95 % EtOH). After excess stain was removed by washing with 100 % ethanol, slides were incubated for 5 min in Histoclear, drained and mounted using DPX. Sections were viewed and imaged with a Leica DMRB microscope. Images were used to estimate leaf width, vein density, quantification of each vein type (lateral, rank1 intermediates and rank 2 intermediates) and also bundle sheath cells length and number.

RNA sequencing, transcript quantification and differential expression

Seeds of segregating T_1 *Zmtml1tml2* were genotyped by seed chipping prior to being germinated on vermiculite. Maize shoot apices were dissected 7 d after germination. Dissected shoot apices were immediately kept in RNAlater™ Stabilization Solution (Invitogen™, Cat. No. AM7020) for preservation prior to RNA extraction. Tissue samples were rinsed with Ambion® nuclease-free water (Invitogen™, Cat. No. AM9932) prior to flash-freezing in liquid nitrogen. Tissue was ground in individual 2 mL Eppendorf tubes with 3 RNAse-free steel balls using a Qiagen TissueLyser set at 30 s bursts of 28 Hz.

Total RNA was extracted from individual shoot apices using the Qiagen RNeasy Plant Mini Kit (Cat. No. 74904). Subsequent DNase treatment was done using the Ambion® TURBO DNA-free™ Kit (Cat. No. AM1907). RNA quantity was checked and normalized using a Qubit™ RNA HS Assay Kit (Cat. No. Q32852). RNA quality was assessed with an Agilent RNA 6000 Nano Kit (Cat. No. 5067-1511) ensuring that all RNA used for library preparation had a RIN value ^{3} 9.0. Strand-specific RNA sequencing library preparation and sequencing was conducted by the Oxford Genomics Centre at the Wellcome Centre for Human Genetics (funded by Wellcome Trust grant reference 203141/A/16/Z) using a TruSeq stranded mRNA library kit. Sequencing was performed on an Illumina NovSeq6000 with paired-end (PE) 150 bp reads. Each transcriptome is a biological replicate from individual shoot apices of 3 different *Zmtml1tml2* seedlings and 3 different genotypically segregating wild-type siblings. Sequencing technical replicates were obtained by sequencing each library twice in a different flowcell.

RNA-Seq raw data quality was checked by FASTQC and summarized by MultiQC.[102] Sequenced reads were mapped to the Zea Mays B73 RefGen V4 genome (https://phytozome-next.jgi.doe.gov/info/Zmays_RefGen_V4) using STAR.[103] Transcript quantification was done with Salmon[104] and differential gene expression was determined using DESEq2.[105] The identification of differentially expressed genes was based on having log 2-fold change (L2FC) ±1, with an adjusted p-value < 0.05.

Differential expression data sub-setting and enrichment analysis

A subset of genes that were differentially expressed between *Zmtml1tml2* plants and genotypically segregating wild-type siblings were classified as transcription factors using the Grassius Maize Transcription Factor Database (https://grassius.org/browsefamily/Maize/TF) annotations. Lists of B73 RefGen V4 gene IDs belonging to each specific transcription factor family were downloaded and cross-referenced with the differentially expressed gene list using a combination of R scripts based on tidyverse and dplyr.[79] Genes known to have a role in auxin and cytokinin pathways were compiled and curated from searches of both the literature[98] and databases (AmiGo knowledgebase,[106] PANTHER[107] and UniProt[108]) using the search words "auxin" or "cytokinin". These lists were also cross-referenced with the differentially expressed gene list using a combination of R scripts, as mentioned above. The distribution of the differentially expressed genes for the specific categories: transcription factor family, and inclusion in the auxin or cytokinin pathway were plotted in R using ggplot2.[78]

Enrichment analysis

Statistical overrepresentation test (ORA) of Gene Ontology annotation set "GO biological process complete" was performed using the PANTHER 17.0 GO Ontology database version (https://doi.org/10.5281/zenodo.7942786 Released 2023-05-10) with a Fisher's Exact test type and a false discovery rate correction. The reference list used comprised of all significantly differentially expressed genes between the *Zmtml1tml2* plants and genotypically segregating wild-type siblings. The significantly up-regulated (L2FC > 1; padj <0.05) and significantly down-regulated (L2FC < 1; padj <0.05) datasets were tested separately. An independent ORA was also done using the subset of the differentially expressed genes between *Zmtml1tml2* plants and genotypically segregating wild-type siblings that were classified as transcription factors using the Grassius Maize Transcription Factor Database.[109] The reference list for this analysis comprised of all significantly differentially expressed genes between the *Zmtml1tml2* plants and segregating wild-type siblings. Enriched child GO terms that were overrepresented at FDR < 0.005 and a corrected P value of $\leq$ 0.05 were plotted in R using ggplot2.[78]

QUANTIFICATION AND STATISTICAL ANALYSIS

Leaf fragment width and bundle sheath cell length were measured using the using the ImageJ software package. Veins were quantified across the whole leaf width and included the midvein.

To estimate total number of BS cell per 5 mm^2 leaf area, information from both paradermal and transverse sections were used. The number of BS cells surrounding each vein type was estimated in wild type and mutant leaves transverse sections (Figure 6H) and paradermal sections were used to estimate BS cell length per vein type in each background (Figure 6G). To obtain total BS cell number per mm leaf length, the total number of each vein type was multiplied with the average number of BS cells surrounding it and with the number of BS cells accompanying the vein found in 1 mm leaf length. Values obtained for each vein types were added then together to obtain the total number of BS cells. The total number of BS cell per 5 mm^2 leaf area was derived from the above calculations. First values per mm^2 leaf area were obtained by diving to total leaf width (mm) and the resulting value multiplied by 5 gave the total number of BS cells per 5 mm^2 leaf area (see Data S5).

Statistical tests were undertaken using R Studio (www.rstudio.com). One-way ANOVA tests were performed for analyses involving more than two groups, followed by Tukey's HSD post-hoc testing if the ANOVA p value was < 0.05. Raw phenotypic data and details of statistical tests are summarized in Data S5.